Magnetic moments of $A = 3$ nuclei obtained from chiral effective field theory operators

Soham Pal,[1,*] Shiplu Sarker[1], Patrick J. Fasano[2,†] Pieter Maris,[1] James P. Vary[1],
Mark A. Caprio[2], and Robert A. M. Basili[3]

[1]*Department of Physics and Astronomy, Iowa State University, Ames, Iowa 50011-3160, USA*
[2]*Department of Physics and Astronomy, University of Notre Dame, Notre Dame, Indiana 46556-5670, USA*
[3]*Department of Electrical and Computer Engineering, Iowa State University, Ames, Iowa 50011-3160, USA*

Chiral effective field theory (χEFT) provides a framework for obtaining internucleon interactions in a systematically improvable fashion from first principles, while also providing for the derivation of consistent electroweak current operators. In this work, we apply consistently derived interactions and currents towards calculating the magnetic dipole moments of the $A = 3$ systems ^{3}H and ^{3}He. We focus here on LENPIC interactions obtained using semilocal coordinate-space (SCS) regularization. Starting from the momentum-space representation of the LENPIC χEFT vector current, we derive the SCS-regularized magnetic dipole operator up through next-to-next-to-leading order (N^{2}LO). We then carry out no-core shell-model calculations for ^{3}H and ^{3}He systems using the SCS LENPIC interaction at N^{2}LO in χEFT and evaluate the magnetic dipole moments obtained using the consistently derived one-nucleon and two-nucleon electromagnetic currents. As anticipated by prior results with χEFT currents, the current corrections through N^{2}LO provide improved, but not yet complete, agreement with experiment for the ^{3}H and ^{3}He magnetic dipole moments.

I. INTRODUCTION

Chiral effective field theory (χEFT) is a systematically improvable approach to obtain internucleon interactions and corresponding electroweak current operators from first principles [1–4]. Multiple implementations of χEFT have emerged that differ in the choice of the subnuclear degrees of freedom, power counting scheme, and choice of regulators. This has led to several internucleon interactions that accurately describe nucleon-nucleon scattering data and the deuteron bound state. Under each such implementation of χEFT, corresponding electroweak current operators may be derived, subject to various challenges in obtaining consistency [5].

The present work is focused on the next stage in the process, where we apply consistently derived interactions and currents towards calculating nuclear physics observables. Historically, corrections to the naive electroweak operators were obtained phenomenologically from meson-exchange theory [6,7]. The program of developing electroweak currents from χEFT was initiated in the context of hybrid approaches which combined phenomenological internucleon interactions with incomplete χEFT currents [8–12].

A new generation of χEFT interactions, and their corresponding currents, have been derived from χEFT by constructing effective operators which act only on nucleonic degrees of freedom, either by the method of unitary transformations (UTs) [13,14] or by means of time-ordered perturbation theory (TOPT) [1–3]. For the Norfolk χEFT potentials [15,16], which are local and include Δ intermediate states, the energy-dependence resulting from the application of TOPT is removed through an inverse T-matrix approach [17,18]. For the potentials of the Low Energy Nuclear Physics International Collaboration (LENPIC) [19–21], which are nonlocal and include only pion intermediate states, operators acting purely on nucleonic degrees of freedom are constructed using the UT method [14,22].

In this work, we apply consistently derived interactions and currents towards calculating the magnetic dipole moments of the $A = 3$ systems ^{3}H and ^{3}He. The magnetic dipole moments of these systems have previously been calculated using χEFT currents, both in hybrid approaches with phenomenological potentials [12,23,24], and in a fully χEFT approach using the Norfolk potentials and currents [25]. We focus here on LENPIC interactions obtained using semilocal coordinate-space (SCS) regularization, developed to preserve the approximately local nature of the long-range potentials and associated currents. We calculate the magnetic dipole moments using wave functions obtained by no-core shell-model (NCSM) [26] calculations. We use the SCS regularized two-nucleon (2N) and two-nucleon plus three-nucleon (2N + 3N) LENPIC potentials up to next-to-next-to-leading order (N^{2}LO), with the consistently derived single-nucleon (1N) and 2N electromagnetic currents. Consequences of applying a similarity renormalization group (SRG) transformation [27–29] to the potential are also considered. Initial results were reported in Ref. [30].

We first derive the SCS-regularized magnetic dipole operator starting from the momentum-space representation of the LENPIC χEFT vector current (Sec. II). We then detail the calculational scheme used for our NCSM calculations of

---

magnetic dipole moments for the $A = 3$ systems (Sec. III), and present our results for the magnetic dipole moments obtained with the LENPIC SCS-regulated interaction and χEFT magnetic dipole operator through N^2LO (Sec. IV). We discuss the effects of including the $3N$ interaction and of the choice of SCS regulator parameter and SRG evolution and compare with prior results. To achieve a compact presentation, we include most of the formal developments regarding the derivation of the SCS-regularized operators in Appendices.

II. MAGNETIC DIPOLE OPERATOR FROM χEFT

The magnetic dipole moment, characterizing the interaction between a charged current and the electromagnetic field, is defined classically as [31]

$$\boldsymbol{\mu} = \frac{1}{2} \int_{\mathbb{R}^3} d^3x \, \mathbf{x} \times \bar{\mathbf{j}}(\mathbf{x}), \tag{1}$$

where $\bar{\mathbf{j}}(\mathbf{x})$ is the charged-current density at position $\mathbf{x}$. We can also express the magnetic dipole moment in terms of the current density in momentum space via the Fourier transform,

$$\bar{\mathbf{j}}(\mathbf{x}) = \int_{\mathbb{R}^3} \frac{d^3k}{(2\pi)^{3/2}} \, e^{i\mathbf{k}\cdot\mathbf{x}} \mathbf{j}(\mathbf{k}), \tag{2}$$

obtaining

$$\boldsymbol{\mu} = \frac{1}{2i} \nabla_{\mathbf{k}} \times \mathbf{j}(\mathbf{k}) \Big|_{\mathbf{k}=0}. \tag{3}$$

If we take the momentum-space matrix element of the nonrelativistic current operator [32] for a charged particle with spin, we obtain

$$\mathbf{j}(\mathbf{p}', \mathbf{p}; \mathbf{k}) = 2\mu_N \left(g_l \frac{\mathbf{p}' + \mathbf{p}}{2} - i g_s \mathbf{k} \times \mathbf{s} \right), \tag{4}$$

with the connection to the quantum-mechanical matrix element given by

$$\langle \mathbf{p}' | \mathbf{j}(\mathbf{k}) | \mathbf{p} \rangle \stackrel{\text{def}}{=} \mathbf{j}(\mathbf{p}', \mathbf{p}; \mathbf{k}) \delta^3(\mathbf{p}' - \mathbf{p} - \mathbf{k}), \tag{5}$$

following the notation of Ref. [33], where $\mu_N = e/2m_N$ is the nuclear magneton, $\mathbf{p}$ ($\mathbf{p}'$) is the initial (final) momentum, $\mathbf{s}$ is the spin operator, g_l and g_s are the orbital and spin g factors, and the momentum eigenstates are normalized as $\langle \mathbf{p}' | \mathbf{p} \rangle = \delta^{(3)}(\mathbf{p}' - \mathbf{p})$. Combining this with (3) and writing the orbital angular momentum $\mathbf{l} = -\mathbf{p} \times i\nabla_{\mathbf{p}}$ in momentum space, we get the conventional [34,35] (impulse-approximation) expression for the magnetic dipole moment operator[1]

$$\boldsymbol{\mu}^{\text{IA}} = \mu_N(g_l \mathbf{l} + g_s \mathbf{s}), \tag{6}$$

where $\mathbf{l}$ and $\mathbf{s}$ are the orbital and spin angular-momentum operators, respectively. The operator $\boldsymbol{\mu}^{\text{IA}}$ is a one-body operator which corresponds to the treatment of nucleons as point particles with charges and intrinsic magnetic moments.

---

[1]The magnetic dipole operator $\boldsymbol{\mu}$ considered here, normalized appropriately for calculation of the magnetic dipole moment, is related to the magnetic dipole operator $\mathbf{M}_1$ found in the theory of electromagnetic transitions (see Appendix A 2) by a conventional factor, as $\boldsymbol{\mu} = (4\pi/3)^{1/2}\mathbf{M}_1$.

For the present work, we have used the LENPIC SCS-regulated potentials described in Refs. [19,20,36], and previously used for low-energy nuclear structure calculations in Refs. [36–38]. The $2N$ potentials have been derived up to next-to-next-to-next-to-next-to leading order (N^4LO) in the chiral order and fit to nucleon-nucleon scattering data and the deuteron bound state, while the $3N$ interactions have been derived up to N^2LO and fit to nucleon-deuteron (Nd) scattering.

Because iteration of the $2N$ interaction with the Lippmann-Schwinger equation generates ultraviolet (UV) divergences [39,40], one must regulate the high-momentum (or, equivalently, short-distance) behavior of the interaction. This is usually done by introducing a momentum-space UV cutoff Λ. Choosing a large value for Λ, such as the mass of the ρ meson, results in spurious deeply bound states, while choosing a small cutoff leads to more-pronounced finite-cutoff artifacts (for more details, see Ref. [20]).

To attempt to mitigate finite-cutoff artifacts, in the LENPIC SCS framework, a hybrid regularization scheme has been adopted. The terms in these potentials arising from pion exchange (without contact interactions) have been regularized in coordinate space by multiplying with the coordinate space function

$$f(r) = \left[1 - \exp\left(-\frac{r^2}{R^2} \right) \right]^6, \tag{7}$$

where r is the relative separation between the two nucleons, and R characterizes the cutoff separation. Meanwhile, the contact terms have been regularized in momentum space by multiplying by the nonlocal Gaussian regulator

$$g(p, p') = \exp\left(-\frac{p^2 + p'^2}{\Lambda^2} \right), \tag{8}$$

where p and p' are the magnitudes of the incoming and outgoing relative nucleon momenta, respectively, with the cutoff $\Lambda = 2R^{-1}$. Here we have two sets of interactions, one set with $R = 0.9$ fm and the other with $R = 1.0$ fm.

For consistency with the regularization scheme for the interaction, we must also regularize the operators that arise from the χEFT expansion of the magnetic dipole moment operator. The current-density operator is typically derived and expressed in momentum space [5,32,41]. However, in order to apply the regulator function in (7), we must transform the long-range parts of the magnetic dipole moment operator to coordinate space. For the coordinate-space matrix element of the a-body operator $\boldsymbol{\mu}^{aN}$ we have [34,42]

$$\boldsymbol{\mu}^{aN}(\mathbf{r}'_1, \ldots, \mathbf{r}'_a, \mathbf{r}_1, \ldots, \mathbf{r}_a)$$
$$= \frac{1}{2} \int d^3x \, \mathbf{x} \times \bar{\mathbf{j}}^{aN}(\mathbf{r}'_1, \ldots, \mathbf{r}'_a, \mathbf{r}_1, \ldots, \mathbf{r}_a; \mathbf{x}), \tag{9}$$

where $\mathbf{r}_i$ ($\mathbf{r}'_i$) is the initial (final) position of the ith nucleon. We define the coordinate-space matrix element of $\bar{\mathbf{j}}^{aN}$ via

$$\langle \mathbf{r}'_1 \cdots \mathbf{r}'_a | \bar{\mathbf{j}}(\mathbf{x}) | \mathbf{r}_1 \cdots \mathbf{r}_a \rangle = \bar{\mathbf{j}}(\mathbf{r}'_1, \ldots, \mathbf{r}'_a, \mathbf{r}_1, \ldots, \mathbf{r}_a; \mathbf{x}). \tag{10}$$

To use the (momentum-space) current matrix elements derived in Refs. [41] and [32] with the coordinate-space regulators, we perform the change of basis via the multidimensional Fourier transform

$$\bar{\mathbf{j}}^{aN}(\mathbf{r}'_1, \ldots, \mathbf{r}'_a, \mathbf{r}_1, \ldots, \mathbf{r}_a; \mathbf{x})$$

$$= \int_{\{\mathbf{q}\}_1^a} \int_{\{\mathbf{Q}\}_1^a} \int_{\mathbf{k}} \prod_{i=1}^a e^{i\mathbf{q}_i \cdot (\mathbf{r}'_i + \mathbf{r}_i)/2}\, e^{i\mathbf{Q}_i \cdot \Delta\mathbf{r}_i}\, e^{i\mathbf{k}\cdot\mathbf{x}}$$

$$\langle \mathbf{p}'_1 \cdots \mathbf{p}'_a | \mathbf{j}(\mathbf{k}) | \mathbf{p}_1 \cdots \mathbf{p}_a \rangle = (2\pi)^{-3a+3} \delta^{(3)}(\mathbf{q}_1 + \cdots + \mathbf{q}_a - \mathbf{k})\mathbf{j}(\mathbf{q}_1, \ldots, \mathbf{q}_a, \mathbf{Q}_1, \ldots, \mathbf{Q}_a; \mathbf{k}), \tag{12}$$

where we adopt the nonrelativistic normalization of states $\langle \mathbf{p}' | \mathbf{p} \rangle = \delta^{(3)}(\mathbf{p}' - \mathbf{p})$. We also use the notations $\int_{\{\mathbf{q}\}_1^a} = \int_{\mathbf{q}_1} \cdots \int_{\mathbf{q}_a}$, with $\int_{\mathbf{q}} = \int \frac{d^3q}{(2\pi)^{3/2}}$, and $\Delta\mathbf{r}_i = \mathbf{r}'_i - \mathbf{r}_i$. From equations (9) and (11) we obtain

$$\boldsymbol{\mu}^{aN}(\ldots)$$

$$= \frac{(2\pi)^3}{2i} \left[\boldsymbol{\nabla}_{\mathbf{k}} \times \int_{\{\mathbf{q}\}_1^a} \int_{\{\mathbf{Q}\}_1^a} \prod_{i=1}^a e^{i\mathbf{q}_i \cdot (\mathbf{r}'_i + \mathbf{r}_i)/2}\, e^{i\mathbf{Q}_i \cdot \Delta\mathbf{r}_i}\, \mathbf{j}^{aN}(\ldots) \right.$$

$$\left. \times\ \delta^{(3)}(\mathbf{q}_1 + \cdots + \mathbf{q}_a - \mathbf{k}) \right]_{\mathbf{k}=0}, \tag{13}$$

where for brevity we have omitted the arguments of $\boldsymbol{\mu}^{aN}$ and $\mathbf{j}^{aN}$.

We use these relations to derive the magnetic dipole operators from the corresponding momentum-space electromagnetic currents. While we will now focus on specific $1N$ and $2N$ currents, we emphasize that this relation is true for any electromagnetic current derived from χEFT. For a general derivation of electric and magnetic multipole operators see Appendix A.

A. Single-nucleon magnetic dipole operators

For $1N$ currents, after integrating over $\mathbf{q}_1$ and expanding the curl, equation (13) reduces to

$$\boldsymbol{\mu}^{1N} = \frac{1}{2i} \left[\frac{i}{2}(\mathbf{r}'_1 + \mathbf{r}_1) \times \int_{\mathbf{Q}_1} e^{i\mathbf{Q}_1 \cdot \Delta\mathbf{r}_1}\, \mathbf{j}^{1N}(\mathbf{q}_1 = \mathbf{k}, \mathbf{Q}_1) \right.$$

$$\left. + \int_{\mathbf{Q}_1} e^{i\mathbf{Q}_1 \cdot \Delta\mathbf{r}_1}\, \boldsymbol{\nabla}_{\mathbf{k}} \times \mathbf{j}^{1N}(\mathbf{q}_1 = \mathbf{k}, \mathbf{Q}_1) \right]_{\mathbf{k}=0}. \tag{14}$$

If the current is independent of $\mathbf{Q}_1$ then integrating over $\mathbf{Q}_1$ gives an additional δ function, $\delta^{(3)}(\Delta\mathbf{r}_1)$. Up to N^{2}LO in the power counting scheme established in Ref. [32], there are two $1N$ currents—one at next-to-leading order (NLO), and the other at N^{2}LO. The $1N$ current at NLO is

$$\mathbf{j}^{1N}_{\text{NLO}} = \frac{e}{4m_N}\left[-i\mathbf{q}_1 \times \boldsymbol{\sigma}_1(g_s + g_v\tau_1^3) + 2\mathbf{Q}_1(1 + \tau_1^3) \right], \tag{15}$$

$$\times\ \mathbf{j}^{aN}(\mathbf{q}_1, \ldots, \mathbf{q}_a, \mathbf{Q}_1, \ldots, \mathbf{Q}_a; \mathbf{k})$$

$$\times\ (2\pi)^{-3a+3}\delta^{(3)}(\mathbf{q}_1 + \cdots + \mathbf{q}_a - \mathbf{k}), \tag{11}$$

where $\mathbf{q}_i = \mathbf{p}'_i - \mathbf{p}_i$, $\mathbf{Q}_i = (\mathbf{p}'_i + \mathbf{p})/2$ are linear combinations of the incoming ($\mathbf{p}_i$) and outgoing ($\mathbf{p}'_i$) momenta of the ith nucleon, and $\mathbf{k}$ is the momentum of the external electromagnetic field. Following the convention of Refs. [32,33], we define the function $\mathbf{j}^{aN}(\mathbf{q}_1, \ldots, \mathbf{q}_a, \mathbf{Q}_1, \ldots, \mathbf{Q}_a; \mathbf{k})$ in terms of the momentum-space matrix element

where m_N is the average nucleon mass, $g_s = \frac{1}{2}(g_{s,p} + g_{s,n})$, and $g_v = \frac{1}{2}(g_{s,p} - g_{s,n})$ are the isoscalar and isovector g factors of the nucleon, respectively, while $\boldsymbol{\sigma}$ and $\boldsymbol{\tau}$ are the Pauli matrices in spin and isospin spaces, respectively. Substituting this current into equation (14) we get

$$\boldsymbol{\mu}^{1N}_{\text{NLO}} = \frac{\mu_N}{2}\left[(g_s + g_v\tau_1^3)\boldsymbol{\sigma}_1 + (1 + \tau_1^3)\mathbf{l}_1 \right]\delta^{(3)}(\Delta\mathbf{r}_1), \tag{16}$$

where $\Delta\mathbf{r}_1 = \mathbf{r}'_1 - \mathbf{r}_1$. This expression is equivalent to $\boldsymbol{\mu}^{\text{IA}}$ in equation (6). The $1N$ current at N^{2}LO, which arises due to the chiral expansion of the $1N$ form factors, is given by

$$\mathbf{j}^{1N}_{\text{N}^2\text{LO}} = -\frac{ieg_A^2}{32\pi F_\pi^2}\tau_1^3\left[m_\pi - (4m_\pi^2 + q_1^2)A(|\mathbf{q}_1|) \right](\mathbf{q}_1 \times \boldsymbol{\sigma}_1), \tag{17}$$

where $A(q) = \frac{1}{2q}\tan^{-1}(\frac{q}{m_\pi})$, g_A is the axial coupling constant, m_π is the average pion mass, and F_π is the pion-decay constant. The chiral expansion of the $1N$ form factors converges slowly, and so in this work we use physical values of the $1N$ form factors, which at $\mathbf{k} = 0$ are just the isoscalar and isovector magnetic moments in equation (15). This current does not contribute to the magnetic dipole moment operator, as can be shown by substituting $\mathbf{j}^{1N}_{\text{N2LO}}$ into equation (13) to obtain zero.

B. Two-nucleon magnetic moment operators

We define the initial relative and center-of-mass coordinates for a $2N$ system:

$$\mathbf{r}_{12} = \mathbf{r}_1 - \mathbf{r}_2, \quad \mathbf{R}_{12} = (\mathbf{r}_1 + \mathbf{r}_2)/2. \tag{18}$$

The final relative and center-of-mass coordinates are similarly defined with $\mathbf{r}'_1$ and $\mathbf{r}'_2$. For $2N$ currents, after expressing the nucleon coordinates in terms of these new coordinates, integrating over $\mathbf{q}_2$, and expanding the curl, equation (13) reduces to

$$\boldsymbol{\mu}^{2N} = \frac{1}{2i}\left[\frac{i}{2}(\mathbf{R}'_{12} + \mathbf{R}_{12}) \int_{\mathbf{q}} \int_{\{\mathbf{Q}\}_1^2} e^{i\mathbf{q}\cdot(\mathbf{r}'_{12}+\mathbf{r}_{12})/2} e^{i(\mathbf{Q}_1+\mathbf{Q}_2)\cdot\Delta\mathbf{R}_{12}} e^{i(\mathbf{Q}_1-\mathbf{Q}_2)\cdot\Delta\mathbf{r}_{12}/4}\mathbf{j}^{2N}\left(\tfrac{1}{2}\mathbf{k} + \mathbf{q}, \tfrac{1}{2}\mathbf{k} - \mathbf{q}, \mathbf{Q}_1, \mathbf{Q}_2\right) \right.$$

$$\left. + \int_{\mathbf{q}} \int_{\{\mathbf{Q}\}_1^2} e^{i\mathbf{q}\cdot(\mathbf{r}'_{12}+\mathbf{r}_{12})/2} e^{i(\mathbf{Q}_1+\mathbf{Q}_2)\cdot\Delta\mathbf{R}_{12}} e^{i(\mathbf{Q}_1-\mathbf{Q}_2)\cdot\Delta\mathbf{r}_{12}/4} \boldsymbol{\nabla}_{\mathbf{k}} \times \mathbf{j}^{2N}\left(\tfrac{1}{2}\mathbf{k} + \mathbf{q}, \tfrac{1}{2}\mathbf{k} - \mathbf{q}, \mathbf{Q}_1, \mathbf{Q}_2\right) \right]_{\mathbf{k}=0}, \tag{19}$$

where we have replaced $\mathbf{q}_1 \to \frac{1}{2}\mathbf{k} + \mathbf{q}$ and $\mathbf{q}_2 \to \frac{1}{2}\mathbf{k} - \mathbf{q}$ in the arguments to the current $\mathbf{j}^{2N}$, while $\Delta\mathbf{r}_{12} = \mathbf{r}'_{12} - \mathbf{r}_{12}$ and $\Delta\mathbf{R}_{12} = \mathbf{R}'_{12} - \mathbf{R}_{12}$. If the current is independent of $\mathbf{Q}_1$ and $\mathbf{Q}_2$ then we get additional δ functions, $\delta^{(3)}(\Delta\mathbf{R}_{12})\delta^{(3)}(\Delta\mathbf{r}_{12})$.

Up to N^2LO there is one $2N$ current, arising from the seagull and pion-in-flight diagrams at NLO [41]:

$$\mathbf{j}_{NLO}^{2N} = \frac{ieg_A^2}{4F_\pi^2}[\boldsymbol{\tau}_1 \times \boldsymbol{\tau}_2]^3 \frac{\boldsymbol{\sigma}_2 \cdot \mathbf{q}_2}{q_2^2 + m_\pi^2}\left(\mathbf{q}_1 \frac{\boldsymbol{\sigma}_1 \cdot \mathbf{q}_1}{q_1^2 + m_\pi^2} - \boldsymbol{\sigma}_1\right)$$
$$+ 1 \leftrightharpoons 2. \tag{20}$$

Using (19) we get the associated magnetic dipole operator

$$\boldsymbol{\mu}_{NLO}^{2N} = g_\pi[\boldsymbol{\tau}_1 \times \boldsymbol{\tau}_2]^3\big[\boldsymbol{\mu}_{NLO,cm\text{-}dep}^{2N}(\mathbf{R}_{12}, \mathbf{r}_{12})$$
$$+ \boldsymbol{\mu}_{NLO,cm\text{-}indep}^{2N}(\mathbf{r}_{12})\big]\delta^{(3)}(\Delta\mathbf{R}_{12})\delta^{(3)}(\Delta\mathbf{r}_{12}), \tag{21}$$

where the center-of-mass dependent part is

$$\boldsymbol{\mu}_{NLO,cm\text{-}dep}^{2N}(\mathbf{R}_{12}, \mathbf{r}_{12})$$
$$= \hat{\mathbf{R}}_{12} \times \hat{\mathbf{r}}_{12}(m_\pi R_{12})Y_0(z)$$
$$\times [Y_2(z)\boldsymbol{\sigma}_1 \cdot \hat{\mathbf{r}}_{12}\,\boldsymbol{\sigma}_2 \cdot \hat{\mathbf{r}}_{12} - Y_1(z)\boldsymbol{\sigma}_1 \cdot \boldsymbol{\sigma}_2], \tag{22}$$

and the center-of-mass independent part is

$$\boldsymbol{\mu}_{NLO,cm\text{-}indep}^{2N}(\mathbf{r}_{12})$$
$$= [(1+z)(\boldsymbol{\sigma}_1 \times \boldsymbol{\sigma}_2) \cdot \hat{\mathbf{r}}_{12}\hat{\mathbf{r}}_{12} - z(\boldsymbol{\sigma}_1 \times \boldsymbol{\sigma}_2)]Y_0(z), \tag{23}$$

where a hat on a symbol denotes a unit vector, $g_\pi = -\frac{2m_N}{e}\frac{eg_A^2 m_\pi}{32\pi F_\pi^2}$, $Y_2(z) = z + \frac{3}{z} + 3$, $Y_1(z) = 1 + \frac{1}{z}$, $Y_0(z) = \frac{e^{-z}}{z}$, and $z = m_\pi r_{12}$.

Finally, given these expressions for the magnetic dipole moment operator in coordinate space, we can apply the regulator scheme consistent with the interaction. Since there are no contact terms in these currents we only need to multiply these coordinate-space expressions by the regulator $f(r_{12}/R)$ from (7). In Appendix B we demonstrate the consistency of the SCS-regularized current.

Note that these operators are written involving products of the basic vector operators $\hat{\mathbf{r}}_{12}$, $\boldsymbol{\sigma}_1$, and $\boldsymbol{\sigma}_2$. To calculate two-body matrix elements of these operators, it is advantageous to carry out angular-momentum recoupling on these products to break these operators into spherical tensor components with definite total orbital angular momentum L and definite total spin angular momentum S. We have provided such tensor decompositions in Appendix C.

III. NO-CORE SHELL-MODEL CALCULATIONS FOR THE THREE-NUCLEON SYSTEM

The $A = 3$ ground-state wave functions, for which we deduce magnetic dipole moments in the present work, are obtained from *ab initio* no-core shell-model (NCSM) [26,43] calculations with the LENPIC interactions. In the NCSM approach we start with an A-body Hamiltonian of the

form

$$H = \frac{1}{2m_N A}\sum_{i<j}^A (\mathbf{p}_i - \mathbf{p}_j)^2$$
$$+ \sum_{i<j}^A V_{2N,ij} + \sum_{i<j<k}^A V_{3N,ijk} + \cdots, \tag{24}$$

where the terms on the right-hand side are the relative kinetic energy, $2N$ interactions, and $3N$ interactions, respectively. The many-body nuclear wave functions $|\Psi\rangle$ are the eigenstates of this Hamiltonian, obtained by solving the A-body Schrödinger equation:

$$H|\Psi\rangle = E|\Psi\rangle, \tag{25}$$

where E is the energy eigenvalue corresponding to the state $|\Psi\rangle$.

The wave functions are expanded in a complete orthonormal basis $\{|\Phi\rangle\}$, where the basis states $|\Phi\rangle$ are Slater determinants of single-particle states $|\phi\rangle$ occupied by the system's nucleons, with fixed parity and fixed total angular-momentum projection. That is,

$$|\Phi\rangle = \mathcal{A}\left[\prod_{i=1}^A |\phi_{\alpha_i}\rangle\right], \tag{26}$$

where the label α_i denotes the quantum numbers of nucleon i, and $\mathcal{A}$ is the antisymmetrization operator. The three-dimensional harmonic oscillator (HO) basis, characterized by the energy parameter $\hbar\omega$, is the conventional choice for the single-particle basis, which we adopt here.

The resulting many-body basis $\{|\Phi\rangle\}$ is, in principle, infinite, but, for actual calculations, we must truncate it. In the usual N_{max} truncation scheme, configurations are selected by limiting the total number of HO quanta, shared among the nucleons, to N_{max}, relative to the minimum number of quanta required by the Pauli principle. This truncation scheme, in particular, ensures a well-behaved center-of-mass wave function (e.g., Ref. [44]).

Expressed in terms of the many-body basis, the A-body Schrödinger equation (25) becomes a finite-dimensional matrix eigenproblem, where the matrix elements of the Hamiltonian are defined as $\langle\Phi_\nu|H|\Phi_\mu\rangle$ with μ and ν labeling the many-body basis states. The exact result, corresponding to the full, untruncated many-body problem, is recovered in the limit $N_{max} \to \infty$. Furthermore, given a large enough N_{max} the expectation value of an observable computed in these bases will approach independence of $\hbar\omega$. We use the MANY FERMION DYNAMICS FOR NUCLEONS (MFDn) package [45,46] to solve this matrix eigenvalue problem and obtain the ground-state energies and corresponding many-body wave functions of the $3N$ systems. We then compute the magnetic dipole moment $\mu(J)$ for these many-body state wave functions, using the magnetic dipole moment operator $\boldsymbol{\mu}$ considered above in Sec. II.[2]

---

[2]In terms of this operator, the magnetic dipole moment $\mu(J)$ [35] of a many-body state of angular momentum J is defined as the

For the $A = 3$ nuclei, calculations can readily be carried out to sufficiently high $N_{\max}$, with the LENPIC $2N$ potentials, to yield the magnetic dipole moment with a numerical precision which is effectively unlimited. However, the present calculations are also intended to explore the use of χEFT currents with the NCSM in anticipation of future application throughout the range of nuclei accessible to the NCSM. In general, the accessible $N_{\max}$ may be expected to critically limit precision which can be obtained for magnetic dipole observables.

Although the χEFT interaction at N^{2}LO includes $3N$ contributions, incorporating these $3N$ into NCSM calculations adversely impacts the sparsity of the many-body Hamiltonian matrix in the NCSM basis, typically imposing an order-of-magnitude penalty in computational demands [48]. Thus, the sensitivity of the calculated magnetic observables to the $3N$ interaction are not only of physical interest but also of computational interest. We calculate magnetic dipole moments for $A = 3$ wave functions obtained from the N^{2}LO LENPIC interaction, including either only the $2N$ contributions to this interaction (LENPIC $2N$) or also the $3N$ contributions (LENPIC $2N + 3N$).

Furthermore, in calculations for all but the very lightest nuclei, in order to provide reasonable convergence for accessible values of $N_{\max}$, the "bare" LENPIC interaction must typically be softened. This is accomplished by applying a similarity renormalization group (SRG) transformation [27–29,36,49–52]. In the SRG approach, the Hamiltonian in a suitable representation (e.g., here, momentum representation) is evolved to a band-diagonal structure by a continuous unitary transformation $H(\alpha) = U(\alpha)H(\alpha = 0)U^{\dagger}(\alpha)$, where $H(\alpha = 0)$ is the starting Hamiltonian, and α is the flow parameter that characterizes the transformation. Applying this transformation to a Hamiltonian with $2N$ interactions induces $3N$ and higher many-body interactions, although the induced interactions are typically truncated at the $3N$ level. The impact of SRG transformation on calculated dipole moments in NCSM calculations, even if such SRG evolution is not actually necessary in the $A = 3$ case, is thus of interest.

Applying a unitary transformation to the Hamiltonian necessitates that the same transformation be applied to operators for observables. SRG evolution of a $2N$ current operator may be expected to induce $3N$ (and higher many-body) contributions to the current operator as well. Here we restrict ourselves to probing the error incurred by applying a typical SRG transformation ($\alpha \lesssim 0.1$ fm^4) to the Hamiltonian, without considering the induced corrections to the magnetic dipole operator. We carry out calculations in which either the LENPIC $2N$ or LENPIC $2N + 3N$ interactions are SRG evolved, in both cases retaining induced interactions up to $3N$.

Before then extracting a magnetic dipole moment from the resulting wave function, we must specify the values for

---

expectation value $\mu(J) \overset{\text{def}}{=} \langle JJ|\mu_z|JJ\rangle$ of the z component in the stretched ($M = J$) substate. Equivalently, in terms of the reduced matrix element [47] of $\boldsymbol{\mu}$, $\mu(J) = (2J + 1)^{-1/2}(JJ10|JJ)\langle J\|\boldsymbol{\mu}\|J\rangle$, where $(j_1m_1 j_2m_2|JM)$ is a Clebsch-Gordan coefficient.

the masses and LECs that appear in the current operator [see (16), (22), and (23)]. For masses and low-energy constants (LECs) which appear in the expressions both for the potentials [19,20] and for the magnetic dipole operator, we use the values already adopted for the potentials: $m_N = 938.919$ MeV, $m_\pi = 138.03$ MeV, $F_\pi = 92.4$ MeV, and $g_A = 1.29$. For the isoscalar and isovector g factors of the nucleon, we have used $g_s = 0.880$ and $g_v = 4.706$.

IV. RESULTS AND DISCUSSION

Considering first the bare, SRG-unevolved LENPIC $2N$ interaction, convergence patterns are shown in Fig. 1 for the calculated ground-state energy (left), magnetic dipole moment (center), and $2N$ meson exchange current (MEC) correction (right), for both ^{3}H (top) and ^{3}He (bottom). In particular, these calculations are for SCS regulator parameter $R = 1.0$ fm. We carry out these NCSM calculations, for the $2N$ interaction, through $N_{\max} = 18$, with $\hbar\omega$ from 20 to 40 MeV in steps of 4 MeV. Note that the variational minimum of the calculated energies [Fig. 1 (left)] occurs within this range.

Calculated dipole moments are shown [Fig. 1 (center)], as they are obtained with just the $1N$ impulse-approximation (IA) dipole operator (μ^{IA}) or including the $2N$ χEFT corrections as well ($\mu^{\text{IA+MEC}}$). Both of these contributions to the moment arise from terms in the current operator which appear at NLO, while it may be recalled (from Sec. II) that the $1N$ contribution to the current arising at N^{2}LO does not contribute to the magnetic dipole moment. The difference between these curves thus represents the total MEC correction through N^{2}LO [Fig. 1 (right)].

Numerical results for the calculated dipole moments are tabulated in Table I, as obtained at the highest $N_{\max}$ and at the $\hbar\omega$ corresponding to the approximate location of the variational minimum of the ground-state energy on our $\hbar\omega$ mesh starting from 14 MeV. These same values for the calculated dipole moments are summarized graphically in Fig. 2 to facilitate comparison while reading the following discussion.

The approach to numerical convergence in the calculated dipole moment is evinced in Fig. 1 (center), as curves for successive $N_{\max}$ become compressed against each other and as the $\hbar\omega$ dependence tends to decrease for the curves of higher $N_{\max}$. Taking ^{3}H [Fig. 1 (top)] for illustration, at the variational energy minimum ($\hbar\omega \approx 32$ MeV), the IA moments [Fig. 1(b)] for $N_{\max} = 14$ and $N_{\max} = 16$ differ by 0.002 μ_N, and those for $N_{\max} = 16$ and $N_{\max} = 18$ differ by only 0.0009 μ_N. The variation of the IA moment with $\hbar\omega$ at $N_{\max} = 18$, over an interval extending by 4 MeV to each side (28 MeV $\leqslant \hbar\omega \leqslant$ 36 MeV) is 0.0019 μ_N. The basis dependence of the MEC correction [Fig. 1(c)] is similar on an absolute scale (e.g., the calculated corrections for $N_{\max} = 16$ and $N_{\max} = 18$ differ again by 0.0009 μ_N, and at $N_{\max} = 18$ the MEC correction is nearly independent of $\hbar\omega$), and both the IA and MEC contributions thus contribute similarly to the basis dependence of the calculated total (IA + MEC) moment [Fig. 1(b)]. However, the basis dependence of the IA and the MEC correction is such that the combined result, $\mu^{\text{IA+MEC}}$, exhibits a weak but seemingly persistent $\hbar\omega$ dependence over the 20 MeV window shown in Fig. 1 (center), even though
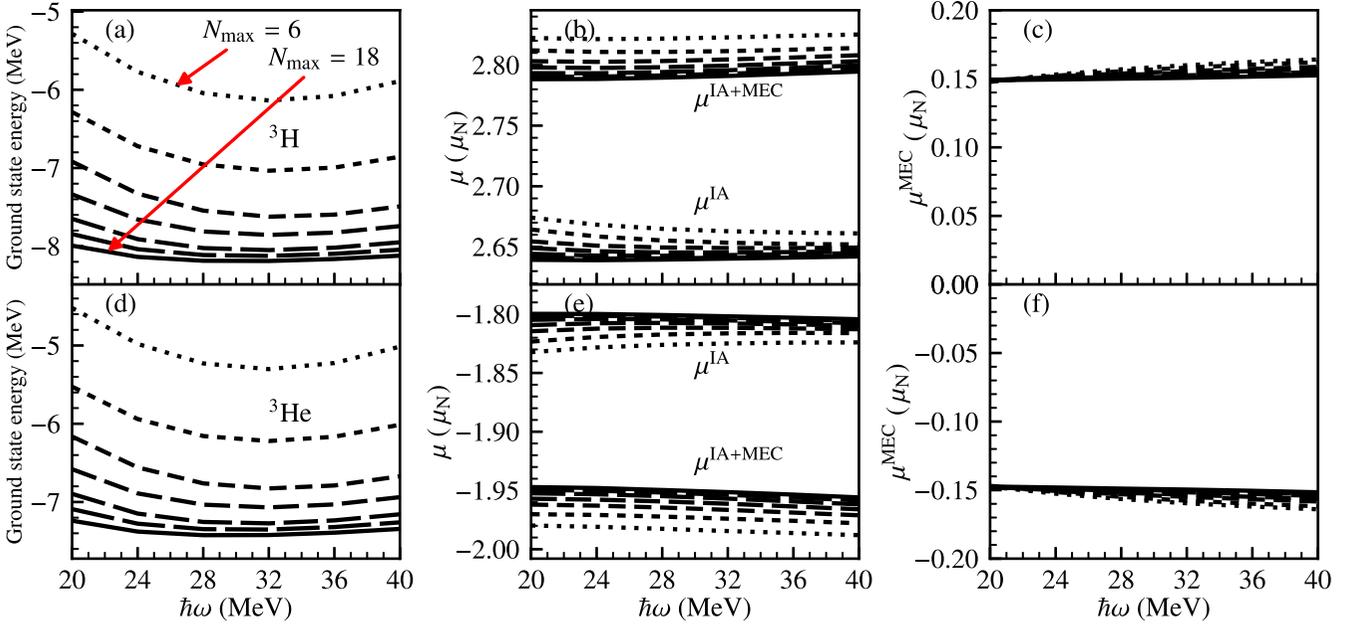
FIG. 1. Calculated ground-state energies (left), magnetic dipole moments (center), and $2N$ MEC corrections (right), for ^{3}H (top) and ^{3}He (bottom), illustrating their convergence with respect to basis parameters N_{max} (successive curves) and $\hbar\omega$. For the magnetic dipole moment, μ^{IA} represents the contribution from the $1N$ impulse approximation (IA) operator $\boldsymbol{\mu}^{1N}$ in Eq. (16), μ^{MEC} represents the contribution from the $2N$ MEC operator $\boldsymbol{\mu}^{2N}$ in Eq. (21), and $\mu^{IA+MEC} = \mu^{IA} + \mu^{MEC}$. Wave functions are obtained using the $2N$ LENPIC SCS potential with $R = 1.0$ fm and no SRG transformation of the potential.

it does seem to converge with N_{max}. We can therefore not put a firm numerical uncertainty on our calculated magnetic moments.

The calculated MEC contributions for the mirror nuclides ^{3}H [Fig. 1(c)] and ^{3}He [Fig. 1(f)] are approximately equal in magnitude (0.15 μ_N) but opposite in sign. This is to be

expected as a consequence of isospin symmetry, given that the sole MEC contribution at NLO may be seen, from the isospin factor in (21), to be manifestly isovector. To facilitate comparison of the pattern of MEC contributions (of approximately equal magnitude but opposite sign) across the mirror nuclides, note that the magnetic dipole moment axis in Fig. 2(b) is

TABLE I. Magnetic moments of the $A = 3$ nuclides calculated with the LENPIC potentials and currents, with consistent LECs, at N^{2}LO (the last nonvanishing contribution to the current thus arises at NLO). The SRG-unevolved LENPIC $2N$ calculations are shown for $N_{max} = 18$, while the other LENPIC calculations are shown for $N_{max} = 14$, with $\hbar\omega$ based on the variational energy minimum. Estimated uncertainties from basis truncation are discussed in the text. Prior results obtained with INOY ($\Lambda = 500$ MeV and 900 MeV) [23], AV18 + IL7 [24], and Norfolk (NV2 + 3-IIb*) [25] potentials, with the χEFT current taken to NLO, are shown for comparison, as are the experimental values [53]. The SRG parameter α is given in units of fm^4, $\hbar\omega$ is in units of MeV, and the magnetic moment in units of μ_N.

				^{3}H			^{3}He		
Potential	R (fm)	α	$\hbar\omega$	μ^{IA}	μ^{MEC}	μ^{IA+MEC}	$\hbar\omega$	μ^{IA}	μ^{MEC}	μ^{IA+MEC}
LENPIC $2N$	0.9	0.00	36	2.629	0.173	2.802	36	−1.796	−0.172	−1.968
	1.0	0.00	32	2.640	0.151	2.791	28	−1.801	−0.149	−1.950
LENPIC $2N$	1.0	0.04	20	2.677	0.143	2.820	16	−1.822	−0.141	−1.963
+ induced $3N$	1.0	0.08	14	2.692	0.139	2.831	14	−1.831	−0.138	−1.969
LENPIC $2N$ + $3N$	1.0	0.04	20	2.667	0.147	2.814	20	−1.817	−0.145	−1.962
	1.0	0.08	14	2.683	0.142	2.825	14	−1.827	−0.141	−1.968
INOY (NLO; 500 MeV)[a]				2.657	0.103	2.760		−1.810	−0.103	−1.913
INOY (NLO; 900 MeV)[a]				2.657	0.172	2.829		−1.810	−0.170	−1.980
AV18 + IL7 (NLO)[a]				2.556	0.253	2.809		−1.743	−0.248	−1.991
Norfolk (NLO)[a]				2.588	0.227	2.815		−1.770	−0.224	−1.994
Experiment						2.979				−2.128

[a]The tabulated values for prior calculations are partial results calculated with the χEFT current taken to NLO and thus involve the same diagrams as appear in the current operator used in calculating the present LENPIC results.

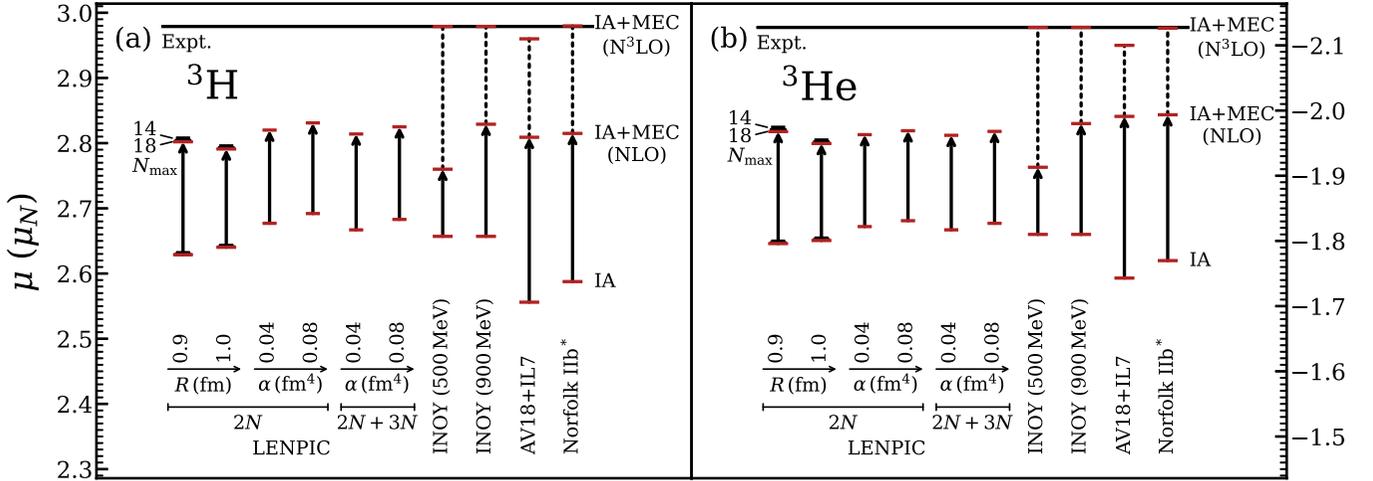FIG. 2. Magnetic moments of the $A = 3$ nuclides (a) ^{3}H and (b) ^{3}He, calculated with the LENPIC potentials and currents, along with results of prior calculations [23–25] (see Table I caption for details of these calculations). Both IA and IA + MEC results are shown (connected by arrow), where the χEFT current contains contributions from terms appearing through NLO. For the prior calculations, results including contributions through N^{3}LO are also shown (connected by dotted line); however, these results involve new LECs which are chosen to replicate (at least approximately) the experimental $A = 3$ moments, and are thus not predictions *per se* (see text). The SRG-unevolved LENPIC $2N$ results are shown for $N_{\rm max} = 14$, 16, and 18 (increasing symbol size), as an indicator of convergence. The SRG-unevolved LENPIC $2N$ results are shown for both $R = 0.9$ fm and $R = 1.0$ fm, while all other LENPIC results are shown for $R = 1.0$ fm. Experimental values [53] are provided for reference (horizontal bars). Note that the magnetic dipole moment axis for ^{3}He (right) is inverted, to facilitate comparison of the pattern of MEC contributions (of approximately equal magnitude but opposite sign, as noted in the text) across mirror nuclides.

inverted. The MEC contribution provides an $\approx 6\%$ correction to the IA moment for ^{3}H, or $\approx 8\%$ for ^{3}He. In each case, the correction serves to increase the magnitude of the moment, providing a positive correction to the positive ^{3}H moment and negative correction to the negative ^{3}He moment.

The experimentally observed dipole moments, for comparison, are 2.979 $\mu_{\rm N}$ for ^{3}H and -2.128 $\mu_{\rm N}$ for ^{3}He [53]. In each case, the IA calculation underpredicts the magnitude of the moment, and the MEC contribution thus has the sign needed to resolve the discrepancy, but the size of the correction is only about half that required to provide agreement with experiment (see Table I and Fig. 2).

Here we may compare with prior results for the $A = 3$ system. Hybrid calculations; that is, with wave functions obtained from phenomenological potentials but moments extracted using χEFT currents, were carried out in Ref. [23] with the INOY $2N$ potential [54], using wave functions obtained from solving the Faddeev equations, and in Ref. [24] with the AV18 + IL7 $2N + 3N$ potentials [55,56], using the Green's function Monte Carlo (GFMC) many-body method [57]. Then, in Ref. [25], fully χEFT calculations with the Norfolk potential and currents were obtained in calculations in a hyperspherical harmonic basis.

These works carry the current operators to N^{3}LO, thus including higher-order contributions than considered in the present work. However, they also provide a detailed breakdown of the contributions to the calculated magnetic moments, arising from terms appearing at different orders in the χEFT current operator. Results obtained by retaining only terms through NLO in the MEC contribution, summarized in Table I and Fig. 2, include the same diagrams as the present MEC results and are thus directly comparable. In the INOY

calculations [23], the IA moments are essentially identical to those found here (to within $\lesssim 0.02$ $\mu_{\rm N}$), and the MEC corrections (at NLO) are comparable in size to those found here (the INOY results obtained for different choices of regulator cutoff Λ bracket the present results). In both the AV18 + IL7 and Norfolk calculations, the IA moment is modestly smaller in magnitude than calculated here (by $\lesssim 0.1$ $\mu_{\rm N}$). However, the NLO correction is correspondingly larger than calculated here, yielding IA + MEC results at NLO closely similar to those obtained here.

The additional MEC contributions appearing up to N^{3}LO in the χEFT currents introduce new LECs, which, in the prior calculations [23–25], were fit so as to reproduce the experimental moments for the $A = 3$ nuclei. Thus, the moments from these calculations [Fig. 2 (dotted lines)] do not constitute predictions *per se* and, indeed, match experiment by construction[3] (the small deviation from experiment in the AV18 + IL7 results arises due to differences in the Hamiltonian, as well as in certain other approximations, between these GFMC calculations and the few-body calculation actually used in fitting the LECs [24]).

Having discussed the qualitative features of the results, let us now examine the sensitivity of the calculated moments in quantitative detail to choices made, first, in the χEFT regulator scheme (Sec. II) and, subsequently, in the calculational process (Sec. III). Comparing calculations with regulator cut-

---

[3]In more recent auxiliary field diffusion Monte Carlo (AFDMC) calculations [58], results with such an approach are, alternatively, contrasted with results for a global fit of the LECs to moments for a selection of light nuclei.

off length scale of $R = 0.9$ fm to those (just considered) with $R = 1.0$ fm induces shifts in the IA moment of $\lesssim 0.006$ μ_N, and changes to the MEC contribution of $\lesssim 0.011$ μ_N (see Table I and Fig. 2). It can easily be understood that the MEC contribution is more sensitive to the regulator scale, because both the wave function and the MEC operator depend on the regulator, whereas the IA operator is independent of the regulator.

Simultaneous SRG evolution of both the interaction and the moment operator, with all induced many-body contributions retained (only operators through $3N$ are relevant in the $A = 3$ system) would leave the results strictly unchanged in the full, untruncated space for the problem. We consider calculations with SRG flow parameter values $\alpha = 0.4$ fm^4 and 0.8 fm^4. Induced interactions are retained through $3N$, but only the unevolved moment operator is used. That is, only the calculated wave functions differ in these calculations, without compensating changes to the operator for the observable. This provides an extreme test of sensitivity to SRG evolution in the calculational scheme. Numerical results are tabulated in Table I for the highest N_{max} calculated, in this case $N_{max} = 14$, again for $\hbar\omega$ at the approximate location of the variational minimum of the ground-state energy on our $\hbar\omega$ mesh for each interaction employed.[4] The resulting changes in the calculated IA moments, as a function of the SRG flow parameter, are $\lesssim 0.05$ μ_N, and the changes in the calculated MEC contribution are $\lesssim 0.012$ μ_N. Note that these changes are of the same order as, or even larger than, the basis dependence shown in Fig. 1 for the unrenormalized magnetic moments.

Finally, inclusion of the $3N$ contributions to the interaction may in general be expected to have significant effects on the structure and on calculated observables [36]. We recalculate the $A = 3$ wave functions using the full LENPIC $2N + 3N$ interaction, again with SRG flow parameter values $\alpha = 0.4$ fm^4 and 0.8 fm^4 (see Table I). However, we find that including the $3N$ interaction appears to have minimal effect ($\lesssim 0.02$ μ_N) on the moments obtained for these wave functions; however, one should keep in mind that the moment operator was not SRG-evolved, and we cannot exclude the possibility that the

---

[4]For the SRG-evolved LENPIC $2N$ and $2N + 3N$ interactions, we carry out the NCSM calculations through $N_{max} = 14$, with $\hbar\omega = 14, 16, 20, 24, 28$, in MeV.

effect of $3N$ interaction is larger when consistent SRG evolved operators are used.

V. SUMMARY

In this work, we calculated the magnetic dipole moments of ^{3}H and ^{3}He with a chirally improved magnetic dipole operator, within the context of the NCSM. Starting from the momentum-space representation of the LENPIC χEFT vector current, we derived the SCS-regularized magnetic dipole operator up to N^{2}LO in chiral order (the methods presented here generalize to higher chiral and multipole orders). We then performed consistent calculations of magnetic dipole moments of these nuclei, with the semilocal coordinate-space regularized LENPIC $2N$ and LENPIC $2N + 3N$ potentials. Here, by a "consistent calculation" we mean that we adopt both the operators and the nuclear potentials up to the same chiral order in the calculation.

This work represents our first step towards consistent calculations of electromagnetic observables using χEFT currents and LENPIC interactions with the NCSM framework. Our results are similar to those of prior theoretical calculations [23–25], when taken with the corresponding NLO current operator, likewise falling short of the experimental values of the magnetic dipole moments of both ^{3}H and ^{3}He by 6%–8%. Including higher-order currents will be essential for a more comprehensive description of nuclear systems (beyond $A = 3$) within the NCSM framework.

APPENDIX A: ELECTROMAGNETIC MULTIPOLE OPERATORS

Here we present a general method to derive all electromagnetic multipole operators from any a-nucleon (aN) charge or current derived from χEFT. This is a generalization of the procedure described in Sec. II. Electric multipole operators are derived from the charge, and magnetic multipole operators are derived from the current.

1. Electric multipole operators

To derive electric multipole operators from an aN charge operator we adopt the following definition [34,42]:

$$\mathbf{E}_{l,}^{aN}(\mathbf{r}_1', \ldots, \mathbf{r}_a', \mathbf{r}_1, \ldots, \mathbf{r}_a) \stackrel{\text{def}}{=} \int d^3\mathbf{x}\, x^l \mathbf{Y}_l(\hat{\mathbf{x}}) \bar{\rho}^{aN}(\mathbf{r}_1', \ldots, \mathbf{r}_a', \mathbf{r}_1, \ldots, \mathbf{r}_a, \mathbf{x}), \tag{A1}$$

where $\bar{\rho}^{aN}$ is the coordinate space representation of the charge, and l is the order of the multipole operator. Note that in this Appendix, and the following Appendix B, we follow the alternative normalization convention of Refs. [41,59] for the expressions for momentum-space matrix elements, in which (12) becomes

$$\langle \mathbf{p}'_1 \cdots \mathbf{p}'_a | \mathbf{j}(\mathbf{k}) | \mathbf{p}_1 \cdots \mathbf{p}_a \rangle = \delta^{(3)}(\mathbf{q}_1 + \cdots + \mathbf{q}_a - \mathbf{k}) \mathbf{j}(\mathbf{q}_1, \ldots, \mathbf{q}_a, \mathbf{Q}_1, \ldots, \mathbf{Q}_a; \mathbf{k}), \tag{A2}$$

and the Fourier transform (11) relating the expressions for momentum-space and coordinate-space matrix elements becomes

$$\bar{\mathbf{j}}^{aN}(\mathbf{r}'_1, \ldots, \mathbf{r}'_a, \mathbf{r}_1, \ldots, \mathbf{r}_a; \mathbf{x}) = \int_{\{\mathbf{q}\}_1^a} \int_{\{\mathbf{Q}\}_1^a} \int_{\mathbf{k}} \prod_{i=1}^{a} e^{i\mathbf{q}_i \cdot (\mathbf{r}'_i + \mathbf{r}_i)/2} \, e^{i\mathbf{Q}_i \cdot \Delta \mathbf{r}_i} \, e^{i\mathbf{k} \cdot \mathbf{x}}$$

$$\times \, \mathbf{j}^{aN}(\mathbf{q}_1, \ldots, \mathbf{q}_a, \mathbf{Q}_1, \ldots, \mathbf{Q}_a; \mathbf{k}) \bar{\delta}^{(3)}(\mathbf{q}_1 + \cdots + \mathbf{q}_a - \mathbf{k}), \tag{A3}$$

where again $\int_{\{\mathbf{q}\}_1^a} = \int_{\mathbf{q}_1} \cdots \int_{\mathbf{q}_a}$, but now with $\int_{\mathbf{q}} = \int \frac{d^3 q}{(2\pi)^3}$, and $\bar{\delta}^{(3)}(\cdots) = (2\pi)^3 \delta^{(3)}(\cdots)$. Then the relation between $\bar{\rho}^{aN}$, and the momentum-space representation ρ^{aN} (derived in Refs. [32,41]) is the same as the relation between $\bar{\mathbf{j}}^{aN}$ and $\mathbf{j}^{aN}$ in equation (A3) above.

We simplify equation (A1) using the following identity [47]:

$$x^l \mathbf{Y}_l(\mathbf{x}) = \sqrt{\frac{(2l + 1)!!}{4\pi l!}} [\cdots [\mathbf{x}\mathbf{x}]_2 \mathbf{x}]_3 \cdots \mathbf{x}]_l. \tag{A4}$$

With this identity Eq. (A1) becomes

$$\mathbf{E}_l^{aN} = (-i)^l \sqrt{\frac{(2l + 1)!!}{4\pi l!}} [[\ldots [\nabla_{\mathbf{k}} \nabla_{\mathbf{k}}]_2 \nabla_{\mathbf{k}}]_3 \ldots \nabla_{\mathbf{k}}]_l$$

$$\times \int_{\mathbf{q}_1 \cdots \mathbf{q}_a} \int_{\mathbf{Q}_1 \cdots \mathbf{Q}_a} \prod_{i=1}^{a} e^{i\mathbf{q}_i \cdot (\mathbf{r}'_i + \mathbf{r}_i)/2} \, e^{i\mathbf{Q}_i \cdot \Delta \mathbf{r}_i} \, \rho^{aN} \bar{\delta}^{(3)}(\mathbf{q}_1 + \cdots + \mathbf{q}_a - \mathbf{k}) \Bigg]_{\mathbf{k}=0}, \tag{A5}$$

where we used $\nabla_{\mathbf{k}} e^{i\mathbf{k} \cdot \mathbf{x}} = i\mathbf{x} e^{i\mathbf{k} \cdot \mathbf{x}}$. The tensor product is interpreted as first applying the $\nabla_{\mathbf{k}}$s to the integral and then extracting the required irreducible tensor component from the result. This is best understood with an example. The electric quadrupole operator, modulo conventional factors, is

$$\mathbf{E}_2^{aN} = -\sqrt{\frac{15}{8\pi}} \left[[\nabla_{\mathbf{k}} \nabla_{\mathbf{k}}]_2 \int_{\mathbf{q}_1 \cdots \mathbf{q}_a} \int_{\mathbf{Q}_1 \cdots \mathbf{Q}_a} \prod_{i=1}^{a} e^{i\mathbf{q}_i \cdot (\mathbf{r}'_i + \mathbf{r}_i)/2} \, e^{i\mathbf{Q}_i \cdot \Delta \mathbf{r}_i} \, \rho^{aN} \bar{\delta}^{(3)}(\mathbf{q}_1 + \mathbf{q}_2 - \mathbf{k}) \right]_{\mathbf{k}=0}. \tag{A6}$$

The leading order (LO) $1N$ charge is $\rho_{\mathrm{LO}}^{1N}(\mathbf{q}_1, \mathbf{Q}_1, \mathbf{k}) = (e/2)(1 + \tau_1^3)(2\pi)^3 \delta^{(3)}(\mathbf{q}_1 - \mathbf{k})$. Substituting this in the above equation gives us

$$\mathbf{E}_{2,\mathrm{LO}}^{1N}(\mathbf{r}'_1, \mathbf{r}_1) = \left(-\sqrt{\frac{15}{8\pi}} [\nabla_{\mathbf{k}} \nabla_{\mathbf{k}}]_2 e^{i\mathbf{k} \cdot \mathbf{r}_1} \Big|_{\mathbf{k}=0} \right) \frac{e}{2} (1 + \tau_1^3) \delta^{(3)}(\mathbf{r}'_1 - \mathbf{r}_1). \tag{A7}$$

Each of the $\nabla_{\mathbf{k}}$ acting on $e^{i\mathbf{k} \cdot \mathbf{r}_1}$ will bring down an $i\mathbf{r}_1$. Extracting the rank-2 irreducible tensor from the resulting tensor we get $\sqrt{15/8\pi} [\mathbf{r}_1 \mathbf{r}_2]_2$, which following equation (A4) is simply $r_1^2 \mathbf{Y}_2(\hat{\mathbf{r}}_1)$. Thus the LO $1N$ electric quadrupole operator is

$$\mathbf{E}_{2,\mathrm{LO}}^{1N}(\mathbf{r}'_1, \mathbf{r}_1) = \frac{e}{2}(1 + \tau_1^3) r_1^2 \mathbf{Y}_2(\hat{\mathbf{r}}_1) \delta^{(3)}(\mathbf{r}'_1 - \mathbf{r}_1), \tag{A8}$$

which is equivalent to the impulse-approximation definition of the electric quadrupole moment operator found in nuclear physics textbooks [34,35].

2. Magnetic multipole operators

Generalizing equation (9) we define the mth spherical component of the rank l magnetic multipole operator as

$$M_{lm,}^{aN}(\mathbf{r}_1, \ldots, \mathbf{r}_a, \mathbf{r}'_1, \ldots, \mathbf{r}_a) \overset{\mathrm{def}}{=} \frac{1}{l + 1} \int d^3 \mathbf{x} [\mathbf{x} \times \bar{\mathbf{j}}^{aN}(\mathbf{r}'_1, \ldots, \mathbf{r}'_a, \mathbf{r}_1, \ldots, \mathbf{r}_a, \mathbf{x})] \cdot \nabla[x^l Y_{lm}(\mathbf{x})], \tag{A9}$$

where $\bar{\mathbf{j}}_O^{aN}$ has been defined in (11), and $Y_{lm}(\mathbf{r})$ is the mth spherical component of $\mathbf{Y}_l(\mathbf{r})$. We use the following identity to simplify this equation [47]:

$$\nabla[x^l Y_{lm}(\mathbf{x})] = \sqrt{l(2l + 1)} x^{l-1} \mathbf{Y}_{lm}^{l-1}(\mathbf{x}), \tag{A10}$$

where $\mathbf{Y}_{lm}^{n}$ is a vector spherical harmonic whose νth spherical component is given by

$$(\mathbf{Y}_{lm}^{n})_{\nu} = (-1)^{\nu} C_{n\,m+\nu\,1\,\nu}^{lm} Y_{n-1\,m-\nu}. \tag{A11}$$

With this identity, Eq. (A4) and the definition of the tensor product equation (A9) becomes

$$M_{lm,}^{aN} = \frac{\sqrt{l(2l+1)}}{l+1} \sqrt{\frac{(2l-1)!!}{4\pi(l-1)!}} \int d^3\mathbf{x} [[[\cdots [\mathbf{x}\mathbf{x}]_2 \mathbf{x}]_3 \cdots \mathbf{x}]_{l-1} [\mathbf{x} \times \bar{\mathbf{j}}^{aN}]]_{lm}, \tag{A12}$$

where for brevity we dropped the arguments of the current. Since this equation is true for all projections m, we can drop the projection index and write the above equation as a tensor equation. Again employing $\nabla_{\mathbf{k}} e^{i\mathbf{k}\cdot\mathbf{x}} = i\mathbf{x} e^{i\mathbf{k}\cdot\mathbf{x}}$ we get the following final form for the magnetic multipole operators:

$$\mathbf{M}_{l,}^{aN} = (-i)^l \frac{\sqrt{l(2l+1)}}{l+1} \sqrt{\frac{(2l-1)!!}{4\pi(l-1)!}} \left\{ \left[\{[[\ldots [\nabla_{\mathbf{k}}\nabla_{\mathbf{k}}]_2 \nabla_{\mathbf{k}}]_3 \ldots \nabla_{\mathbf{k}}]_{l-1}\right] \left[\nabla_{\mathbf{k}} \times \int_{\mathbf{q}_1 \cdots \mathbf{q}_a} \int_{\mathbf{Q}_1 \cdots \mathbf{Q}_a} \prod_{i=1}^{a} e^{i\mathbf{q}_i \cdot (\mathbf{r}_i' + \mathbf{r}_i)/2} e^{i\mathbf{Q}_i \cdot \Delta \mathbf{r}_i} \mathbf{j}^{aN} \right] \right]_l \right\}_{\mathbf{k}=0}. \tag{A13}$$

The interpretation of the tensor products of the $\nabla_{\mathbf{k}}$ is similar to that in the case of the electric multipole operators. We first apply the $\nabla_{\mathbf{k}}$ to the integral and then extract the required irreducible tensor from the result. For $l = 1$, after multiplying by the conventional factor $\sqrt{4\pi/3}$, the above equation reduces to equation (13).

APPENDIX B: CONSISTENCY OF SEMI-LOCAL COORDINATE SPACE OF REGULARIZED CURRENT

The consistency of the current is determined by whether it satisfies the continuity equation

$$\mathbf{k} \cdot \hat{\mathbf{j}} = [\hat{H}, \hat{\rho}] \tag{B1}$$

in momentum space or, equivalently,

$$\nabla_{\mathbf{x}} \cdot \hat{\mathbf{j}} = -i[\hat{H}, \hat{\rho}] \tag{B2}$$

in coordinate space. (In this Appendix, a hat on a symbol denotes an operator.) Here $\hat{j}^{\mu} = \{\hat{\rho}, \hat{\mathbf{j}}\}$ is the four-current operator, $\hat{H} = \hat{T} + \hat{V}$ is the strong part of the nuclear Hamiltonian where $\hat{T}$ denotes the kinetic energy, and $\hat{V} = \hat{V}_{\text{LO}} + \hat{V}_{NLO} + \cdots$ denotes the potential energy, and the divergence is with respect to the position of the external electromagnetic source. As discussed in Refs. [32,60,61], the $1N$ current satisfies the continuity equation with the kinetic energy, and the first $2N$ current at NLO satisfies the continuity equation with the LO unregularized potential energy. We do not regularize the kinetic energy. We just have to check the continuity equation for the $2N$ current.

The momentum space representation of the four-current operator (where, as in Appendix A, we follow the normalization conventions of Refs. [41,59]) is [41]

$$\langle \mathbf{p}_1' \mathbf{p}_2' | \hat{j}^{2N,\mu}(\mathbf{k}) | \mathbf{p}_1 \mathbf{p}_2 \rangle = \delta^{(3)}(\mathbf{q}_1 + \mathbf{q}_2 - \mathbf{k}) j^{2N,\mu}(\mathbf{q}_1, \mathbf{q}_2, \mathbf{Q}_1, \mathbf{Q}_2; \mathbf{k}). \tag{B3}$$

If $j^{aN,\mu}$ does not depend on the $\mathbf{Q}_i$ (as is true for the current under consideration), then the coordinate-space representation is of the form

$$\bar{j}^{2N,\mu}(\mathbf{r}_1', \mathbf{r}_2', \mathbf{r}_1, \mathbf{r}_2; \mathbf{x}) = \langle \mathbf{r}_1' \mathbf{r}_2' | \hat{j}^{2N,\mu}(\mathbf{x}) | \mathbf{r}_1 \mathbf{r}_2 \rangle = \frac{1}{(2\pi)^3} \delta^{(3)}(\mathbf{r}_1' - \mathbf{r}_1) \delta^{(3)}(\mathbf{r}_2' - \mathbf{r}_2) \bar{j}^{2N,\mu}(\mathbf{r}_1, \mathbf{r}_2; \mathbf{x}), \tag{B4}$$

where the relation between $j^{2N,\mu}$ and $\bar{j}^{2N,\mu}$ is the same as for the three-currents in equation (A3). We will use the momentum representation to check the continuity equation for the NLO $2N$ current. The left-hand side of equation (B1) in the momentum representation is

$$\langle \mathbf{p}_1' \mathbf{p}_2' | \mathbf{k} \cdot \hat{\mathbf{j}}_{\text{NLO}}^{2N} | \mathbf{p}_1 \mathbf{p}_2 \rangle = \mathbf{k} \cdot \mathbf{j}_{\text{NLO}}^{2N}(\mathbf{q}_1, \mathbf{q}_2) \delta^{(3)}(\mathbf{q}_1 + \mathbf{q}_2 - \mathbf{k}), \tag{B5}$$

where $\mathbf{j}_{\text{NLO}}^{2N}$ has been defined in equation (20). Doing the dot product, while replacing $\mathbf{k}$ by $\mathbf{q}_1 + \mathbf{q}_2$, we get

$$\mathbf{k} \cdot \mathbf{j}_{\text{NLO}}^{2N} = i \frac{e g_A^2}{4F_\pi^2} (\boldsymbol{\tau}_1 \times \boldsymbol{\tau}_2)_z \left(\frac{\boldsymbol{\sigma}_1 \cdot \mathbf{q}_1 \boldsymbol{\sigma}_2 \cdot \mathbf{q}_1}{q_1^2 + m_\pi^2} - \frac{\boldsymbol{\sigma}_1 \cdot \mathbf{q}_2 \boldsymbol{\sigma}_2 \cdot \mathbf{q}_2}{q_2^2 + m_\pi^2} \right). \tag{B6}$$

To evaluate the right-hand side of (B1) we need the momentum representation of the unregularized LO potential:

$$\langle \mathbf{p}_1' \mathbf{p}_2' | \hat{V}_{\text{LO}} | \mathbf{p}_1 \mathbf{p}_2 \rangle = V_{\text{LO}}\left(\tfrac{1}{2}(\mathbf{p}_1' - \mathbf{p}_2' - \mathbf{p}_1 + \mathbf{p}_2)\right) \delta^{(3)}(\mathbf{p}_1' + \mathbf{p}_2' - \mathbf{p}_1 - \mathbf{p}_2), \tag{B7}$$

where $V_{\text{LO}}(\mathbf{q})$ is given by

$$V_{\text{LO}}(\mathbf{q}) = \boldsymbol{\tau}_1 \cdot \boldsymbol{\tau}_2 W_{1\pi}(\mathbf{q}) = -\frac{g_A^2}{4F_\pi^2} \boldsymbol{\tau}_1 \cdot \boldsymbol{\tau}_2 \frac{\boldsymbol{\sigma}_1 \cdot \mathbf{q} \, \boldsymbol{\sigma}_2 \cdot \mathbf{q}}{q^2 + m_\pi^2}. \tag{B8}$$

Now we can evaluate what will be the momentum space representation of $\hat{V}_{\mathrm{LO}}\hat{\rho}_{\mathrm{LO}}$:

$$
\langle \mathbf{p}'_1 \mathbf{p}'_2 | \hat{V}_{\mathrm{LO}} \hat{\rho}_{\mathrm{LO}} | \mathbf{p}_1 \mathbf{p}_2 \rangle = \int d^3 \mathbf{p}''_1 d^3 \mathbf{p}''_2 \, \langle \mathbf{p}'_1 \mathbf{p}'_2 | \hat{V}_{\mathrm{LO}} | \mathbf{p}''_1 \mathbf{p}''_2 \rangle \, \langle \mathbf{p}''_1 \mathbf{p}''_2 | \hat{\rho}_{\mathrm{LO}} | \mathbf{p}_1 \mathbf{p}_2 \rangle
$$

$$
= \int d^3 \mathbf{p}''_1 d^3 \mathbf{p}''_2 \, V_{\mathrm{LO}}\big(\tfrac{1}{2}(\mathbf{p}'_1 - \mathbf{p}'_2 - \mathbf{p}''_1 + \mathbf{p}''_2)\big)\delta^{(3)}(\mathbf{p}'_1 + \mathbf{p}'_2 - \mathbf{p}''_1 - \mathbf{p}''_2)
$$

$$
\times \, [\rho_{\mathrm{LO},1}\delta^{(3)}(\mathbf{p}''_1 + \mathbf{p}''_2 - \mathbf{p}_1 - \mathbf{p}_2 - \mathbf{k})\delta^{(3)}(\mathbf{p}''_2 - \mathbf{p}_2) + (1 \leftrightarrow 2)]. \tag{B9}
$$

Completing the integrals over $\mathbf{p}''_1$, and $\mathbf{p}''_2$, we get

$$
\langle \mathbf{p}'_1 \mathbf{p}'_2 | \hat{V}_{\mathrm{LO}} \hat{\rho}_{\mathrm{LO}} | \mathbf{p}_1 \mathbf{p}_2 \rangle = [V_{\mathrm{LO}}(\mathbf{q}_1)\rho_{\mathrm{LO},1} + (1 \leftrightarrow 2)]\delta^{(3)}(\mathbf{q}_1 + \mathbf{q}_2 - \mathbf{k}), \tag{B10}
$$

where $\rho_{\mathrm{LO},i} = e(1 + \tau_i^3)/2$. We can similarly evaluate $\hat{\rho}_{\mathrm{LO}}\hat{V}_{\mathrm{LO}}$. Using the commutation relation $[\boldsymbol{\tau}_1 \cdot \boldsymbol{\tau}_2, \tau_1^3] = 2i(\boldsymbol{\tau}_1 \times \boldsymbol{\tau}_2)^3$ we see that

$$
\langle \mathbf{p}'_1 \mathbf{p}'_2 | [\hat{V}_{\mathrm{LO}}, \hat{\rho}_{\mathrm{LO}}] | \mathbf{p}_1 \mathbf{p}_2 \rangle = ([V_{\mathrm{LO}}(\mathbf{q}_1), \rho_{\mathrm{LO},1}] + (1 \leftrightarrow 2))\delta^{(3)}(\mathbf{q}_1 + \mathbf{q}_2 - \mathbf{k})
$$

$$
= i \frac{e g_A^2}{4 F_\pi^2}(\boldsymbol{\tau}_1 \times \boldsymbol{\tau}_2)^3 \left(\frac{\boldsymbol{\sigma}_1 \cdot \mathbf{q}_1 \boldsymbol{\sigma}_2 \cdot \mathbf{q}_1}{q_1^2 + m_\pi^2} - \frac{\boldsymbol{\sigma}_1 \cdot \mathbf{q}_2 \boldsymbol{\sigma}_2 \cdot \mathbf{q}_2}{q_2^2 + m_\pi^2} \right)\delta^{(3)}(\mathbf{q}_1 + \mathbf{q}_2 - \mathbf{k}). \tag{B11}
$$

Thus $\langle \mathbf{p}'_1 \mathbf{p}'_2 | \mathbf{k} \cdot \hat{\mathbf{j}}_{\mathrm{NLO}}^{2N} | \mathbf{p}_1 \mathbf{p}_2 \rangle = \langle \mathbf{p}'_1 \mathbf{p}'_2 | [\hat{V}_{\mathrm{LO}}, \hat{\rho}_{\mathrm{LO}}] | \mathbf{p}_1 \mathbf{p}_2 \rangle$, i.e., the NLO $2N$ current satisfies the continuity equation with the unregularized LO potential [32,60,61]. Fourier transforming both sides of this equation we get the continuity equation satisfied by the current in coordinate space, $\langle \mathbf{r}'_1 \mathbf{r}'_2 | \boldsymbol{\nabla}_{\mathbf{x}} \cdot \hat{\mathbf{j}}_{\mathrm{NLO}}^{2N} | \mathbf{r}_1 \mathbf{r}_2 \rangle = -i \langle \mathbf{r}'_1 \mathbf{r}'_2 | [\hat{V}_{\mathrm{LO}}, \hat{\rho}_{\mathrm{LO}}] | \mathbf{r}_1 \mathbf{r}_2 \rangle$, where

$$
\langle \mathbf{r}'_1 \mathbf{r}'_2 | \boldsymbol{\nabla}_{\mathbf{x}} \cdot \hat{\mathbf{j}}_{\mathrm{NLO}}^{2N} | \mathbf{r}_1 \mathbf{r}_2 \rangle = \boldsymbol{\nabla}_{\mathbf{x}} \cdot \bar{\mathbf{j}}_{\mathrm{NLO}}^{2N}(\mathbf{r}_1, \mathbf{r}_2, \mathbf{x})\delta^{(3)}(\mathbf{r}'_1 - \mathbf{r}_1)\delta^{(3)}(\mathbf{r}'_2 - \mathbf{r}_2) \tag{B12}
$$

$$
\langle \mathbf{r}'_1 \mathbf{r}'_2 | \hat{V}_{\mathrm{LO}}(\mathbf{r}_1, \mathbf{r}_2) | \mathbf{r}_1 \mathbf{r}_2 \rangle = \boldsymbol{\tau}_1 \cdot \boldsymbol{\tau}_2 \bar{W}_{1\pi}(\mathbf{r}_1 - \mathbf{r}_2)\delta^{(3)}(\mathbf{r}'_1 - \mathbf{r}_1)\delta^{(3)}(\mathbf{r}'_2 - \mathbf{r}_2), \tag{B13}
$$

$$
\langle \mathbf{r}'_1 \mathbf{r}'_2 | \hat{\rho}_{\mathrm{LO}} | \mathbf{r}_1 \mathbf{r}_2 \rangle = e\left(\frac{1 + \tau_{1z}}{2}\delta^{(3)}(\mathbf{r}_1 - \mathbf{x}) + (1 \leftrightarrow 2) \right)\delta^{(3)}(\mathbf{r}'_1 - \mathbf{r}_1)\delta^{(3)}(\mathbf{r}'_2 - \mathbf{r}_2), \tag{B14}
$$

where $\bar{\mathbf{j}}_{\mathrm{NLO}}^{2N}$ and $\bar{W}_{1\pi}$ are the Fourier transforms of $\mathbf{j}_{\mathrm{NLO}}^{2N}$, and $W_{1\pi}$, respectively. With this form for the coordinate space representation we see that

$$
\boldsymbol{\nabla}_{\mathbf{x}} \cdot \bar{\mathbf{j}}_{\mathrm{NLO}}^{2N}(\mathbf{r}_1, \mathbf{r}_2, \mathbf{x}) = e(\boldsymbol{\tau}_1 \times \boldsymbol{\tau}_2)_z \bar{W}_{1\pi}(\mathbf{r}_1 - \mathbf{r}_2)[\delta^{(3)}(\mathbf{r}_1 - \mathbf{x}) - \delta^{(3)}(\mathbf{r}_2 - \mathbf{x})]. \tag{B15}
$$

Introducing a discrete, complete basis, such as the HO basis, we can write this continuity equation as a matrix equation $\mathcal{Z} = \mathcal{W}$, where the matrix elements are

$$
\mathcal{Z}_{\alpha\beta} = \int d^3 \mathbf{r}_1 d^3 \mathbf{r}_2 \, \phi_\alpha(\mathbf{r}_1, \mathbf{r}_2)\boldsymbol{\nabla}_{\mathbf{x}} \cdot \bar{\mathbf{j}}_{\mathrm{NLO}}^{2N}(\mathbf{r}_1, \mathbf{r}_2, \mathbf{x})\phi_\beta(\mathbf{r}_1, \mathbf{r}_2), \tag{B16}
$$

$$
\mathcal{W}_{\alpha\beta} = e(\boldsymbol{\tau}_1 \times \boldsymbol{\tau}_2)_z \int d^3 \mathbf{r}_1 d^3 \mathbf{r}_2 \, [\delta^{(3)}(\mathbf{r}_1 - \mathbf{x}) - \delta^{(3)}(\mathbf{r}_2 - \mathbf{x})]\phi_\alpha(\mathbf{r}_1, \mathbf{r}_2)\bar{W}_{1\pi}(\mathbf{r}_1 - \mathbf{r}_2)\phi_\beta(\mathbf{r}_1, \mathbf{r}_2), \tag{B17}
$$

where $\{|\alpha\rangle = |\alpha_1, \alpha_2\rangle\}$ is the basis, and $\langle \mathbf{r}_1 \mathbf{r}_2 | \alpha \rangle = \phi_\alpha(\mathbf{r}_1, \mathbf{r}_2)$. We now introduce two new operators $\hat{f}$, and $\hat{g}$ such that $\langle \mathbf{r}'_1 \mathbf{r}'_2 | \hat{f} | \mathbf{r}_1 \mathbf{r}_2 \rangle = f(\mathbf{r}_1 - \mathbf{r}_2)\delta^{(3)}(\mathbf{r}'_1 - \mathbf{r}_1)\delta^{(3)}(\mathbf{r}'_2 - \mathbf{r}_2)$, and $\langle \mathbf{r}'_1 \mathbf{r}'_2 | \hat{g} | \mathbf{r}_1 \mathbf{r}_2 \rangle = g(\mathbf{r}_1, \mathbf{r}_2)\delta^{(3)}(\mathbf{r}'_1 - \mathbf{r}_1)\delta^{(3)}(\mathbf{r}'_2 - \mathbf{r}_2)$. Here f, and g are functions of nucleon coordinates, with no isospin structure. It can be easily checked that $\hat{\mathbf{j}}_{\mathrm{NLO}}^{2N}$ commutes with $\hat{g}$, and $\hat{V}_{\mathrm{LO}}$ commutes with $\hat{f}$. We want to see how $\hat{f}$ and $\hat{g}$ are related if we demand that $\boldsymbol{\nabla}_{\mathbf{x}} \cdot (\hat{\mathbf{j}}_{\mathrm{NLO}}^{2N}\hat{g}) = -i[\hat{V}_{\mathrm{LO}}\hat{f}, \hat{\rho}_{\mathrm{LO}}]$. We will use the coordinate-space relations that we have derived above. In the coordinate-space representation, the left-hand side of this equation evaluates to

$$
\langle \mathbf{r}'_1 \mathbf{r}'_2 | \boldsymbol{\nabla}_{\mathbf{x}} \cdot \hat{\mathbf{j}}_{\mathrm{NLO}}^{2N} \hat{g} | \mathbf{r}_1 \mathbf{r}_2 \rangle = \int d^3 \mathbf{x}_1 d^3 \mathbf{x}_2 \, \langle \mathbf{r}'_1 \mathbf{r}'_2 | \boldsymbol{\nabla}_{\mathbf{x}} \cdot \hat{\mathbf{j}}_{\mathrm{NLO}}^{2N} | \mathbf{x}_1 \mathbf{x}_2 \rangle \, \langle \mathbf{x}'_1 \mathbf{x}'_2 | \hat{g} | \mathbf{r}_1 \mathbf{r}_2 \rangle
$$

$$
= \boldsymbol{\nabla}_{\mathbf{x}} \cdot \mathbf{j}_{\mathrm{NLO}}^{2N}(\mathbf{r}_1, \mathbf{r}_2, \mathbf{x})g(\mathbf{r}_1, \mathbf{r}_2)\delta^{(3)}(\mathbf{r}'_1 - \mathbf{r}_1)\delta^{(3)}(\mathbf{r}'_2 - \mathbf{r}_2). \tag{B18}
$$

To evaluate the right-hand side of this equation, in the coordinate space representation, we first need to evaluate $\langle \mathbf{r}'_1 \mathbf{r}'_2 | \hat{V}_{\mathrm{LO}} \hat{f} \hat{\rho}_{\mathrm{LO}} | \mathbf{r}_1 \mathbf{r}_2 \rangle$.

$$
\langle \mathbf{r}'_1 \mathbf{r}'_2 | \hat{V}_{\mathrm{LO}} \hat{f} \hat{\rho}_{\mathrm{LO}} | \mathbf{r}_1 \mathbf{r}_2 \rangle = \int d^3 \mathbf{x}'_1 d^3 \mathbf{x}'_2 d^3 \mathbf{x}_1 d^3 \mathbf{x}_2 \, \langle \mathbf{r}'_1 \mathbf{r}'_2 | \hat{V}_{\mathrm{LO}} | \mathbf{x}'_1 \mathbf{x}'_2 \rangle \, \langle \mathbf{x}'_1 \mathbf{x}'_2 | \hat{f} | \mathbf{x}_1 \mathbf{x}_2 \rangle \, \langle \mathbf{x}_1 \mathbf{x}_2 | \hat{\rho}_{\mathrm{LO}} | \mathbf{r}_1 \mathbf{r}_2 \rangle
$$

$$
= V_{\mathrm{LO}}(\mathbf{r}_1, \mathbf{r}_2)\rho_{\mathrm{LO}}(\mathbf{r}_1, \mathbf{r}_2, \mathbf{x})f(\mathbf{r}_1 - \mathbf{r}_2)\delta^{(3)}(\mathbf{r}'_1 - \mathbf{r}_1)\delta^{(3)}(\mathbf{r}'_2 - \mathbf{r}_2), \tag{B19}
$$

where $V_{\text{LO}}(\mathbf{r}_1, \mathbf{r}_2)$, and $\rho_{\text{LO}}(\mathbf{r}_1, \mathbf{r}_2, \mathbf{x})$, are the expressions in the right-hand side of equations (B12), and (B13), respectively, modulo the δ functions involving $\mathbf{r}'_i$. We can similarly evaluate $\langle \mathbf{r}'_1 \mathbf{r}'_2 | \hat{\rho}_{\text{LO}} \hat{V}_{\text{LO}} \hat{f} | \mathbf{r}_1 \mathbf{r}_2 \rangle$:

$$\langle \mathbf{r}'_1 \mathbf{r}'_2 | [\hat{V}_{\text{LO}} \hat{f}, \hat{\rho}_{\text{LO}}] | \mathbf{r}_1 \mathbf{r}_2 \rangle = e(\boldsymbol{\tau}_1 \times \boldsymbol{\tau}_2)_z \bar{W}_{1\pi}(\mathbf{r}_1 - \mathbf{r}_2)[\delta^{(3)}(\mathbf{r}_1 - \mathbf{x}) - \delta^{(3)}(\mathbf{r}_2 - \mathbf{x})]f(\mathbf{r}_1, \mathbf{r}_2)\delta^{(3)}(\mathbf{r}'_1 - \mathbf{r}_1)\delta^{(3)}(\mathbf{r}'_2 - \mathbf{r}_2). \quad \text{(B20)}$$

Thus according to our demand,

$$\nabla_{\mathbf{x}} \cdot \mathbf{j}^{2N}_{\text{NLO}}(\mathbf{r}_1, \mathbf{r}_2, \mathbf{x})g(\mathbf{r}_1, \mathbf{r}_2)\delta^{(3)}(\mathbf{r}'_1 - \mathbf{r}_1)\delta^{(3)}(\mathbf{r}'_2 - \mathbf{r}_2)$$
$$= e(\boldsymbol{\tau}_1 \times \boldsymbol{\tau}_2)_z \bar{W}_{1\pi}(\mathbf{r}_1 - \mathbf{r}_2)[\delta^{(3)}(\mathbf{r}_1 - \mathbf{x}) - \delta^{(3)}(\mathbf{r}_2 - \mathbf{x})]f(\mathbf{r}_1, \mathbf{r}_2)\delta^{(3)}(\mathbf{r}'_1 - \mathbf{r}_1)\delta^{(3)}(\mathbf{r}'_2 - \mathbf{r}_2). \quad \text{(B21)}$$

Then by equation (B15) we have $\nabla_{\mathbf{x}} \cdot \mathbf{j}^{2N}_{\text{NLO}}(\mathbf{r}_1, \mathbf{r}_2, \mathbf{x})(g(\mathbf{r}_1, \mathbf{r}_2) - f(\mathbf{r}_1 - \mathbf{r}_2)) = 0$, which means if $\nabla_{\mathbf{x}} \cdot \mathbf{j}^{2N}_{\text{NLO}}$ is not zero, then $g(\mathbf{r}_1, \mathbf{r}_2) = f(\mathbf{r}_1 - \mathbf{r}_2)$. In the discrete, complete basis, introduced earlier this translates to

$$\mathcal{Z}\mathcal{G} = \mathcal{W}\mathcal{F}, \quad \text{(B22)}$$

where

$$\mathcal{F}_{\alpha\beta} = \int d^3\mathbf{r}_1 d^3\mathbf{r}_2 \phi_\alpha(\mathbf{r}_1, \mathbf{r}_2)f(\mathbf{r}_1 - \mathbf{r}_2)\phi_\beta(\mathbf{r}_1, \mathbf{r}_2),$$

$$\mathcal{G}_{\alpha\beta} = \int d^3\mathbf{r}_1 d^3\mathbf{r}_2 \phi_\alpha(\mathbf{r}_1, \mathbf{r}_2)g(\mathbf{r}_1, \mathbf{r}_2)\phi_\beta(\mathbf{r}_1, \mathbf{r}_2) \quad \text{(B23)}$$

are the matrices corresponding to $\hat{f}$ and $\hat{g}$, respectively, in the discrete, complete basis. Since $\mathcal{Z} = \mathcal{W}$, if $\mathcal{Z}$ is nonsingular then $\mathcal{G} = \mathcal{F}$, i.e., the matrix elements of the two regulators must be the same. Even though here we derived this result for the $2N$ current at NLO, it is evident that as long as equation (B15) is satisfied for a particular pair of current and unregularized potential, we will reach the same conclusion.

APPENDIX C: TENSOR DECOMPOSITION OF TWO-NUCLEON OPERATORS

We define the rank j tensor product of two irreducible tensors $\mathbf{T}_{j_1}$ and $\mathbf{T}_{j_2}$ of ranks j_1 and j_2, respectively, as

$$[\mathbf{T}_{j_1}\mathbf{T}_{j_2}]^m_j = \sum_{m_1, m_2} C^{jm}_{j_1 m_1 j_2 m_2} T^{m_1}_{j_1} T^{m_2}_{j_2}, \quad \text{(C1)}$$

where m, m_1, and m_2 are the projection indices and $C^{jm}_{j_1 m_1 j_2 m_2}$ is a Clebsch-Gordan coefficient. The tensor product itself is an irreducible tensor. It follows from the above definition and properties of the Clebsch-Gordan coefficients that the following recoupling identities hold for commuting tensors [47]:

$$[\mathbf{T}_a\mathbf{T}_b]_c = (-1)^{a+b-c}[\mathbf{T}_b\mathbf{T}_a]_c, \quad \text{(C2)}$$

$$[[\mathbf{T}_a\mathbf{T}_b]_c\mathbf{T}_d]_e = (-1)^{a+b+d+e}\sum_f \Pi_{cf} \begin{Bmatrix} a & b & c \\ d & e & f \end{Bmatrix} \{\mathbf{T}_a[\mathbf{T}_b\mathbf{T}_d]_f\}_e, \quad \text{(C3)}$$

$$[[\mathbf{T}_a\mathbf{T}_b]_c[\mathbf{T}_d\mathbf{T}_e]_f]_i = \sum_{hi} \Pi_{cfgh} \begin{Bmatrix} a & b & c \\ d & e & f \\ g & h & i \end{Bmatrix} \{[\mathbf{T}_a\mathbf{T}_d]_g[\mathbf{T}_b\mathbf{T}_e]_h\}_i, \quad \text{(C4)}$$

where $\Pi_{ab\cdots\lambda} = \sqrt{(2a+1)(2b+1)\cdots(2\lambda+1)}$, and the quantities in the braces in equations (C3) and (C4) are the Wigner $6j$ and $9j$ symbols, respectively. These identities hold for any projections of the tensor product, hence we have omitted any explicit projection index. Using $\mathbf{T} \cdot \mathbf{S} = -\sqrt{3}[\mathbf{T}_1\mathbf{S}_1]_0$ and $\mathbf{T} \times \mathbf{S} = -i\sqrt{2}[\mathbf{T}_1\mathbf{S}_1]_1$, and the above identities we have

$$(\boldsymbol{\sigma}_1 \times \boldsymbol{\sigma}_2) \cdot \hat{\mathbf{r}}_{12}\hat{\mathbf{r}}_{12} = i\frac{\sqrt{2}}{3}\{\boldsymbol{\Sigma}_1 + \sqrt{10}[\mathbf{C}^2_{2,0}\boldsymbol{\Sigma}_1]_1\}, \quad \text{(C5)}$$

$$\hat{\mathbf{R}}_{12} \times \hat{\mathbf{r}}_{12}\boldsymbol{\sigma}_1 \cdot \boldsymbol{\sigma}_2 = -i\sqrt{6}[\mathbf{C}^1_{1,1}\boldsymbol{\Sigma}_0]_1, \quad \text{(C6)}$$

$$\hat{\mathbf{R}}_{12} \times \hat{\mathbf{r}}_{12}(\boldsymbol{\sigma}_1 \cdot \hat{\mathbf{r}}_{12}\boldsymbol{\sigma}_2 \cdot \hat{\mathbf{r}}_{12}) = i\frac{\sqrt{2}}{3}\left\{-\sqrt{3}[\mathbf{C}^1_{1,1}\boldsymbol{\Sigma}_0]_1 + \sqrt{\frac{3}{5}}[\mathbf{C}^1_{1,1}\boldsymbol{\Sigma}_1]_1 + \sqrt{\frac{9}{5}}[\mathbf{C}^2_{1,1}\boldsymbol{\Sigma}_2]_1 + \sqrt{\frac{14}{5}}[\mathbf{C}^2_{3,1}\boldsymbol{\Sigma}_2]_1 + \sqrt{\frac{24}{5}}[\mathbf{C}^3_{3,1}\boldsymbol{\Sigma}_2]_1\right\}, \quad \text{(C7)}$$

where $\boldsymbol{\Sigma}_l = [\boldsymbol{\sigma}_1\boldsymbol{\sigma}_2]_l$ and $\mathbf{C}^c_{a,b} = [\mathbf{C}_a(\mathbf{r}_{12})\mathbf{C}_b(\mathbf{R}_{12})]_c$. The $\mathbf{C}_l(\mathbf{r}) = \sqrt{4\pi/(2l+1)}\mathbf{Y}_l(\mathbf{r})$ is the rank l renormalized spherical harmonic. We would like to remind the reader that the numerical subscripts associated with the Pauli matrices and the unit vectors represent nucleon indices and not tensor ranks. Combining all of this we can write Eq. (21) as

$$\boldsymbol{\mu}^{2N}_{\text{NLO}} = \frac{2}{3}g_\pi[\boldsymbol{\tau}_1\boldsymbol{\tau}_2]_1[\boldsymbol{\mu}'^{2N}_{\text{NLO,cm-dep}}(\mathbf{R}_{12}, \mathbf{r}_{12}) + \boldsymbol{\mu}'^{2N}_{\text{NLO,cm-indep}}(\mathbf{r}_{12})]\delta^{(3)}(\Delta\mathbf{R}_{12})\delta^{(3)}(\Delta\mathbf{r}_{12}), \quad \text{(C8)}$$

where

$$\boldsymbol{\mu}'^{2N}_{\text{NLO,cm-dep}}(\mathbf{R}_{12}, \mathbf{r}_{12}) = (m_\pi R_{12}) \left[-\sqrt{3} z [\mathbf{C}^1_{1,1} \boldsymbol{\Sigma}_0]_1 + Y_2(z) \left(+\sqrt{\frac{3}{5}} [\mathbf{C}^1_{1,1} \boldsymbol{\Sigma}_1]_1 + \sqrt{\frac{9}{5}} [\mathbf{C}^2_{1,1} \boldsymbol{\Sigma}_2]_1 \right. \right.$$
$$\left. \left. + \sqrt{\frac{14}{5}} [\mathbf{C}^2_{3,1} \boldsymbol{\Sigma}_2]_1 + \sqrt{\frac{24}{5}} [\mathbf{C}^3_{3,1} \boldsymbol{\Sigma}_2]_1 \right) \right] Y_0(z), \tag{C9}$$

and

$$\boldsymbol{\mu}'^{2N}_{\text{NLO,cm-indep}}(\mathbf{r}_{12}) = \sqrt{10}(1+z) [\mathbf{C}^2_{2,0} \boldsymbol{\Sigma}_1]_1 + (-1+2z)\boldsymbol{\Sigma}_1. \tag{C10}$$

[1] S. Weinberg, Phys. Lett. B **251**, 288 (1990).
[2] S. Weinberg, Nucl. Phys. B **363**, 3 (1991).
[3] C. Ordóñez and U. van Kolck, Phys. Lett. B **291**, 459 (1992).
[4] C. Ordóñez, L. Ray, and U. van Kolck, Phys. Rev. Lett. **72**, 1982 (1994).
[5] H. Krebs, Eur. Phys. J. A **56**, 234 (2020).
[6] J. L. Friar, Ann. Phys. (NY) **104**, 380 (1977).
[7] J. L. Friar, Phys. Rev. C **22**, 796 (1980).
[8] T.-S. Park, D.-P. Min, and M. Rho, Phys. Rep. **233**, 341 (1993).
[9] T.-S. Park, D.-P. Min, and M. Rho, Nucl. Phys. A **596**, 515 (1996).
[10] T.-S. Park, K. Kubodeera, D.-P. Min, and M. Rho, Nucl. Phys. A **684**, 101 (2001).
[11] T.-S. Park, L. E. Marcucci, R. Schiavilla, M. Viviani, A. Kievsky, S. Rosati, K. Kubodera, D.-P. Min, and M. Rho, Phys. Rev. C **67**, 055206 (2003).
[12] Y.-H. Song, R. Lazauskas, T.-S. Park, and D.-P. Min, Phys. Lett. B **656**, 174 (2007).
[13] J. A. Eden and M. F. Gari, Phys. Rev. C **53**, 1510 (1996).
[14] E. Epelbaoum, W. Gloeckle, and U.-G. Meißner, Nucl. Phys. A **637**, 107 (1998).
[15] M. Piarulli, L. Girlanda, R. Schiavilla, R. N. Pérez, J. E. Amaro, and E. R. Arriola, Phys. Rev. C **91**, 024003 (2015).
[16] M. Piarulli, L. Girlanda, R. Schiavilla, A. Kievsky, A. Lovato, L. E. Marcucci, S. C. Pieper, M. Viviani, and R. B. Wiringa, Phys. Rev. C **94**, 054007 (2016).
[17] S. Pastore, L. Girlanda, R. Schiavilla, and M. Viviani, Phys. Rev. C **84**, 024001 (2011).
[18] M. Piarulli, L. Girlanda, L. E. Marcucci, S. Pastore, R. Schiavilla, and M. Viviani, Phys. Rev. C **87**, 014006 (2013).
[19] E. Epelbaum, H. Krebs, and U.-G. Meißner, Phys. Rev. Lett. **115**, 122301 (2015).
[20] E. Epelbaum, H. Krebs, and U.-G. Meißner, Eur. Phys. J. A **51**, 53 (2015).
[21] P. Reinert, H. Krebs, and E. Epelbaum, Phys. Rev. Lett. **126**, 092501 (2021).
[22] E. Epelbaum, W. Gloeckle, and U.-G. Meißner, Nucl. Phys. A **671**, 295 (2000).
[23] Y.-H. Song, R. Lazauskas, and T.-S. Park, Phys. Rev. C **79**, 064002 (2009).
[24] S. Pastore, S. C. Pieper, R. Schiavilla, and R. B. Wiringa, Phys. Rev. C **87**, 035503 (2013).
[25] R. Schiavilla, A. Baroni, S. Pastore, M. Piarulli, L. Girlanda, A. Kievsky, A. Lovato, L. Marcucci, S. C. Pieper, M. Viviani, and R. B. Wiringa, Phys. Rev. C **99**, 034005 (2019).

[26] B. R. Barrett, P. Navrátil, and J. P. Vary, Prog. Part. Nucl. Phys. **69**, 131 (2013).
[27] S. D. Głazek and K. G. Wilson, Phys. Rev. D: Part. Fields **48**, 5863 (1993).
[28] S. D. Głazek and K. G. Wilson, Phys. Rev. D: Part. Fields **49**, 4214 (1994).
[29] F. Wegner, Ann. Phys. (Berlin, Ger.) **506**, 77 (1994).
[30] S. Pal, Ph.D. thesis, Iowa State University, 2022 (unpublished).
[31] J. D. Jackson, *Classical Electrodynamics*, 3rd ed. (Wiley, Hoboken, New Jersey, 1999).
[32] H. Krebs, E. Epelbaum, and U.-G. Meißner, Few-Body Syst. **60**, 31 (2019).
[33] H. Krebs, E. Epelbaum, and U.-G. Meißner, Ann. Phys. (NY) **378**, 317 (2017).
[34] A. Bohr and B. R. Mottelson, *Nuclear Structure* (World Scientific Publishing Company, Singapore, 1998).
[35] J. Suhonen, *From Nucleons to Nucleus: Concepts of Microscopic Nuclear Theory*, Theoretical and Mathematical Physics (Springer, Berlin, 2007).
[36] E. Epelbaum, J. Golak, K. Hebeler, T. Hüther, H. Kamada, H. Krebs, P. Maris, U.-G. Meißner, A. Nogga, R. Roth, R. Skibiński, K. Topolnicki, J. P. Vary, K. Vobig, and H. Witała, Phys. Rev. C **99**, 024313 (2019).
[37] S. Binder, A. Calci, E. Epelbaum, R. J. Furnstahl, J. Golak, K. Hebeler, H. Kamada, H. Krebs, J. Langhammer, S. Liebig, P. Maris, U.-G. Meißner, D. Minossi, A. Nogga, H. Potter, R. Roth, R. Skibiński, K. Topolnicki, J. P. Vary, and H. Witała, Phys. Rev. C **93**, 044002 (2016).
[38] S. Binder, A. Calci, E. Epelbaum, R. J. Furnstahl, J. Golak, K. Hebeler, T. Hüther, H. Kamada, H. Krebs, P. Maris, U.-G. Meißner, A. Nogga, R. Roth, R. Skibiński, K. Topolnicki, J. P. Vary, K. Vobig, and H. Witala, Phys. Rev. C **98**, 014002 (2018).
[39] E. Epelbaum and J. Gegelia, Eur. Phys. J. A **41**, 341 (2009).
[40] R. Machleidt and D. R. Entem, Phys. Rep. **503**, 1 (2011).
[41] S. Kölling, E. Epelbaum, H. Krebs, and U.-G. Meißner, Phys. Rev. C **84**, 054008 (2011).
[42] J. Carlson and R. Schiavilla, Rev. Mod. Phys. **70**, 743 (1998).
[43] J. P. Vary, R. Basili, W. Du, M. Lockner, P. Maris, S. Pal, and S. Sarker, Phys. Rev. C **98**, 065502 (2018).
[44] M. A. Caprio, A. E. McCoy, and P. J. Fasano, J. Phys. G **47**, 122001 (2020).
[45] P. Maris, M. Sosonkina, J. P. Vary, E. Ng, and C. Yang, Procedia Comput. Sci. **1**, 97 (2010).
[46] M. Shao, H. M. Aktulga, C. Yang, E. G. Ng, P. Maris, and J. P. Vary, Comput. Phys. Commun. **222**, 1 (2018).

[47] D. A. Varshalovich, A. N. Moskalev, and V. K. Khersonskii, *Quantum Theory of Angular Momentum* (World Scientific Publishing Company, 1988).

[48] P. Maris, H. M. Aktulga, S. Binder, A. Calci, Ü. V. Çatalyürek, J. Langhammer, E. Ng, E. Saule, R. Roth, J. P. Vary, and C. Yang, J. Phys.: Conf. Ser. **454**, 012063 (2013).

[49] S. K. Bogner, R. J. Furnstahl, and R. J. Perry, Phys. Rev. C **75**, 061001(R) (2007).

[50] S. Bogner, R. Furnstahl, P. Maris, R. Perry, A. Schwenk, and J. Vary, Nucl. Phys. A **801**, 21 (2008).

[51] E. D. Jurgenson, P. Navrátil, and R. J. Furnstahl, Phys. Rev. C **83**, 034301 (2011).

[52] E. D. Jurgenson, P. Maris, R. J. Furnstahl, P. Navrátil, W. E. Ormand, and J. P. Vary, Phys. Rev. C **87**, 054312 (2013).

[53] J. E. Purcell and C. G. Sheu, Nucl. Data Sheets **130**, 1 (2015).

[54] P. Doleschall, I. Borbély, Z. Papp, and W. Plessas, Phys. Rev. C **67**, 064005 (2003).

[55] R. B. Wiringa, V. G. J. Stoks, and R. Schiavilla, Phys. Rev. C **51**, 38 (1995).

[56] S. C. Pieper, V. R. Pandharipande, R. B. Wiringa, and J. Carlson, Phys. Rev. C **64**, 014001 (2001).

[57] J. Carlson, S. Gandolfi, F. Pederiva, S. C. Pieper, R. Schiavilla, K. E. Schmidt, and R. B. Wiringa, Rev. Mod. Phys. **87**, 1067 (2015).

[58] J. D. Martin, S. J. Novario, D. Lonardoni, J. Carlson, S. Gandolfi, and I. Tews, Auxiliary field diffusion Monte Carlo calculations of magnetic moments of light nuclei with chiral EFT interactions, arXiv:2301.08349.

[59] S. Kölling, E. Epelbaum, H. Krebs, and U. G. Meißner, Phys. Rev. C **80**, 045502 (2009).

[60] D. O. Riska, Prog. Part. Nucl. Phys. **11**, 199 (1984).

[61] S. Pastore, R. Schiavilla, and J. L. Goity, Phys. Rev. C **78**, 064002 (2008).